Time-Resolved Resonance Raman and Density Functional Theory Study of Hydrogen-Bonding Effects on the Triplet State of *p*-Methoxyacetophenone

Wing Sum Chan, Chensheng Ma, Wai Ming Kwok, and David Lee Phillips*

Department of Chemistry, The University of Hong Kong, Pokfulam Road, Hong Kong S. A. R., People's Republic of China

Received: December 1, 2004; In Final Form: February 3, 2005

Picosecond and nanosecond time-resolved resonance Raman spectroscopy combined with density functional theory calculations have been performed to characterize the structure, dynamics, and hydrogen-bonding effects on the triplet state of the phototrigger model compound *p*-methoxyacetophenone (MAP) in cyclohexane, MeCN, and 50% H_2O/50% MeCN (v:v) mixed solvent. Analogous work has also been done to study the corresponding ground state properties. The ground and triplet states of MAP were both found to be associated strongly with the water solvent molecules in the 50% H_2O/50% MeCN solvent system. A hydrogen-bond complex model involving one or two water molecules bonded with the oxygen atoms of the MAP carbonyl and methoxy moieties has been employed to explore the hydrogen-bond interactions and their influence on the geometric and electronic properties for the ground and triplet states of MAP. Among the various hydrogen-bond configurations examined, the carbonyl hydrogen-bond configuration involving one water molecule was calculated to lead to the most stable hydrogen-bond complex for both the ground and the triplet states with the strength of the hydrogen-bond interaction being stronger in the triplet state than the ground state. The increased carbonyl located hydrogen-bond strength in the triplet state results in substantial modification of both the electronic and the structural conformation so that the triplet of the hydrogen-bond complex can be considered as a distinct species from the free MAP triplet state. This provides a framework to interpret the differences observed in the TR^3 spectral and triplet lifetime obtained in the neat MeCN solvent (attributed to the free MAP triplet state) and the 50% H_2O/50% MeCN solvent (due to the triplet of the hydrogen-bond complex). Temporal evolution at early picosecond times indicates rapid ISC conversion, and subsequent relaxation of the excess energy of the initially formed energetic triplets occurs for both the free MAP and the hydrogen-bond complex. The triplet of the carbonyl hydrogen-bond complex appears to be generated directly from the corresponding ground state complex and it does not dissociate back to the free triplet state within the triplet state lifetime. We briefly discuss the influence of the carbonyl hydrogen-bond effect on the $\pi\pi^*$ triplet reactivity for MAP and closely related compounds.

Introduction

Photochemically removable protecting groups are becoming increasingly important in time-resolved studies of biochemical processes, multistep syntheses, combinatorial chemistry, and photolithographic technology.[1−8] These protecting groups are also named caged molecules or phototriggers in terms of their biochemical applications.[1−4] Among various protecting groups, aromatic α-keto groups, especially the *p*-hydroxyphenacyl (*p*HP) and *p*-methoxyphenacyl (*p*MP) compounds, have received much attention due to their potential use as efficient phototriggers for the liberation of various biological stimulants.[1−6] Previous work on *p*HP[3,4a,6] and *p*MP[1,3c,4a,8] found that the photochemistry of the two compounds is highly solvent sensitive but depends differently on the solvent properties. Photoreaction of *p*HP phototriggers occurs exclusively in aqueous or largely aqueous containing solvents leading to the release of the protected groups and a *p*-hydroxyphenylacetic rearranged product.[3,4a,6] Photodeprotection of the *p*MP compounds, on the other hand, exhibits more complicated solvent dependence and results in a complex product distribution with a low efficiency for deprotection.[1,3c,6,8] In particular, the *p*MP caged acetate was found to be nonreactive in the 50% H_2O/50% MeCN (v:v) mixed solvent, in contrast to the efficient photorelease reaction of *p*HP caged acetate observed under the same experimental conditions.[3,6] The apparently similar configuration of the *p*HP and *p*MP cages but the different photochemistry of the corresponding phototriggers renders them as ideal compounds to make a comparison for the mechanistic study of the photodeprotection pathways.[1,3,4a,6] Knowledge of the role of water in aqueous solutions is essential to understand the *p*HP and *p*MP deprotection mechanism. Although this issue has been studied in several previous works[1,3,4a,6] and valuable information has been obtained, the overall photoexcited reaction pathway is still not well-established, and there remain conflicting interpretations about the deprotection mechanism.

By employing a combination of femtosecond Kerr gated time-resolved fluorescence (KTRF) and picosecond and nanosecond time-resolved resonance Raman (TR^3) spectroscopy, we have recently studied the early time photophysics of *p*HP phototriggers and the parent compound *p*-hydroxyacetophenone (HA) in neat MeCN and 50% H_2O/50% MeCN (v:v) mixed solutions.[9,10] These studies reveal that the intersystem crossing (ISC) is rapid with the triplet formation occurring at a rate of $\sim 5 \times 10^{11}$ s^{-1} in both the solvent systems. It was also found that the

* To whom correspondence should be addressed. E-mail: Phillips@hku.hk; fax: 852-2857-1586.

10.1021/jp044546+ CCC: $30.25
Published on Web 03/26/2005

triplet state lifetime is leaving group dependent and became remarkably shorter in the water mixed solvent as compared to neat MeCN. This indicates that the triplet is likely the reactive precursor for the *p*HP photorelease reaction.[10] To elucidate the reaction step(s) after the generation of the triplet and the role of water in assisting the reaction, we have performed a comparative study on the corresponding *p*MP phototrigger and parent compound MPA. In this paper, our TR^3 results for MAP in neat MeCN and H_2O/MeCN mixed solvent show that there is rapid formation of the triplet state in both the solvent systems, similar to that of the *p*HP compounds.[9,10] However, it was unexpected that the lifetime of the triplet became noticeably longer in the water mixed MeCN solvent system than in the neat MeCN solvent. In addition, when comparing the triplet TR^3 spectra recorded in the two solvents, we found that there were substantial frequency shifts for many Raman bands and some differences in the appearance of the spectra. This appears to indicate there is noticeable modification of the triplet structure by a specific triplet solute−solvent hydrogen-bonding (H-bonding) interaction that is expected to exist only in the water mixed solvent but absent in the neat MeCN solvent. However, the lifetime lengthening seems puzzling since many solute−solvent H-bonding leads to a shortening of the excited-state lifetime by introducing accepting vibrational modes to facilitate nonradiative depopulation processes.[11,12] Interpretation of this interesting experimental observation is essential with regard to the significance of water involved in the phenacyl photodeprotection chemistry. This requires a comprehensive understanding of the MAP triplet configuration and how the surrounding solvent property, especially the H-bonding interaction, influences it.

We note in this aspect that, besides the photodeprotection related background, MAP has long been taken as a prototypical representative for aromatic carbonyl (AC) compounds with a $\pi\pi^*$ triplet.[13−19] The H-bonding interaction between the MAP triplet (as a H-bond acceptor) and the solvent water molecule(s) (as a H-bonding donor) is expected because of the well-known fact that the carbonyl groups of AC compounds become more nucleophilic in the $\pi\pi^*$ triplet state than in their ground state.[20−26] Extensive investigations on photoexited AC compounds reported in the literature indicate the general importance of the excited-state H-bonding interaction and have pointed out that the H-bonding is one of the key factors in controlling the photophysical and photochemical pathway for most AC compounds.[12,20−31] For instance, it was found that, depending on the kinds of compounds, introducing the solute−solvent H-bonding can enhance or inhibit the rate of ISC (to triplet) and/or IC (to ground state) to deactivate the initial photopopulated singlet exited state.[20,29,30] There have been many studies that have reported different triplet chemical reactivity in water containing solvent systems as compared to organic solvent systems, and these differences have been mostly associated with the triplet H-bond interaction with solvent water molecule(s), although no explicit solid evidence has been presented.[12,21,27,28,31] The profound H-bonding effects have been mostly attributed to the shifts (sometimes inverse) of electronic levels due to the destabilization of the $n\pi^*$ states and stabilization of the $\pi\pi^*$ states. Although earlier investigations have demonstrated a strong correlation of the excited-state electronic property ($n\pi^*$ vs $\pi\pi^*$) to specific H-bonding interactions, studies on the excited state structural changes caused by the H-bonding are rare. This is probably due to the fact that most of the relevant studies were done using transient absorption,[12,23,26−31] fluorescence,[20,29a] and phosphorescence[21,22,24,25] measurements that contain little detailed structural information.

On the basis of the triplet reactivity and phosphorescence profile, location, and lifetime, the MAP triplet has been assigned consistently in previous studies to have a $\pi\pi^*$ nature that is insensitive to solvent properties.[13,15−18] In this context, the different TR^3 results we obtained for the MAP triplet in MeCN and H_2O/MeCN mixed solvents may indicate the presence of structural modification resulting from H-bonding interactions. Here, we report a combined picosecond and nanosecond TR^3 experimental and density functional theory (DFT) study on the geometric and electronic configuration for the H-bonded MAP triplet state and its comparison with the free MAP triplet state. We also performed Raman experiments and DFT calculations for the corresponding ground states to obtain a better understanding of changes in structure and H-bonding topology upon going from the ground state to the triplet state.

Vibrational spectroscopy (Raman and IR) to characterize the solute−solvent H-bonding interaction has been well-demonstrated for many ground-state systems,[32−35] but only a few excited-state H-bond systems[11,36,37] have been studied using these methods. TR^3 spectroscopy provides a vibrational spectrum and therefore structural information about the excited-state species. The differences in the TR^3 spectrum for the H-bonded excited species obtained in a H-bond donating solvent (50% H_2O/50% MeCN here) from that of a nonbonded species recorded in an aprotic solvent (MeCN here) can reveal information about the H-bonding topologies. The frequency shifts for the relevant vibrational modes and their spectral variations are sensitive to the site-specific H-bond effect. Theoretical calculations for the molecular complex containing the solute molecule of interest and a necessary amount of solvent molecules has been found to afford reasonable models that can be used to explain different experimental results obtained in different solvents.[38−44,45] The DFT results presented here are based on a H-bond complex model containing one MAP molecule and one or two water molecules H-bonded with the methoxy and carbonyl oxygen lone pairs. The calculations are meant to provide theoretical information on the possible geometries and frequencies of vibrational modes for both the ground and the triplet states of the free MAP and the MAP H-bonded complexes. The calculations also provide binding energies for the H-bonded complexes. By comparing the theoretical and experimental results, the actual geometry for the free MAP and MAP H-bonded complexes has been identified for both the ground and the triplet states. It can be seen that this complex model provides a reasonable framework for the interpretation of the experimental observations, and our results show that the H-bonding leads to significant modification for both the geometric and the electronic configurations of the MAP triplet. This could consequently influence the MAP triplet reactivity. We briefly discuss the H-bonding effects in relation to the triplet reactivity for the *p*HP and *p*MP photorelease processes and other relevant reactions that have been reported in previous studies.

Experimental and Computational Methods

Normal Raman spectra of the MAP ground state were obtained with a 532 nm excitation wavelength provided by the second harmonic of a Nd:YAG laser. The excitation energy was ~7 mJ with a repetition rate of 10 Hz. The laser beam was focused loosely onto a thin film stream of a recirculated solution with a sample concentration of ~0.1 M. The Raman light was collected in a backscattering configuration and detected by a liquid nitrogen-cooled CCD. The normal Raman spectra pre-

sented were obtained from subtraction of appropriately scaled solvent spectra from the corresponding sample spectra.

The ns-TR^3 experiments were done using a 266 nm pump wavelength and a 416 nm probe wavelength. The pump laser pulse came from the fourth harmonic of the Nd:YAG Q-switched laser, and the probe pulse came from the first Stokes of a hydrogen Raman shifted line pumped by the third harmonic (355 nm) from the second Nd:YAG laser. The energy for the pump and probe pulses were in the range of 2.5−3.5 mJ with a 10 Hz repetition rate. The detection system was the same as that utilized for the normal Raman measurements. The time delay between the pump and the probe pulse was controlled electronically by using a pulse delay generator and was monitored by a photodiode and a 500 MHz oscilloscope. The time resolution of these experiments was ∼10 ns. Spectra with time delays up to 1000 ns were recorded, and the MAP sample concentration was ∼1 mM. Accumulation time for each of the ns-TR^3 spectra displayed was 10 min. The spectra were obtained by subtracting a probe-before-pump spectrum from the corresponding pump−probe spectrum. To check the diffusive quenching effect by oxygen, dynamics measurements were done under open air as well as with nitrogen and oxygen being bubbled through the sample system.

For the ps-TR^3 measurements, the titanium:sapphire regenerative amplifier laser system was operated in picosecond mode with an 800 nm, ∼1 ps, and 1 kHz output. Samples were pumped by a 267 nm laser pulse and probed with a 400 nm laser pulse. The 267 nm pump and 400 nm probe pulses were produced from the third and second harmonic of the regenerative amplifier fundamentals, respectively. The pump and probe pulse durations were ∼1.5 ps with energies of the sample about ∼2−3 μJ. The time delay between the pump and the probe pulses was controlled using an optical delay line with a time resolution of ∼2 ps. The sample handling (∼1.5 mM sample concentration) and signal collecting systems were the same as those used for the ns-TR^3 and normal Raman experiments. The polarization of the pump and probe beams was set at the magic angle and focused to a spot the size of ∼200 μm on the sample. Details of the ps-TR^3 experimental apparatus are given in refs 10, 45, and 46. Each of the ps-TR^3 spectra shown here was accumulated over 2 min with appropriately scaled pump only and probe only spectra being subtracted from a pump−probe spectrum.

MAP is commercially available and was used after recrystallization from MeCN. HPLC-grade solvent MeCN, cyclohexane, and distilled water were used for both the normal and the TR^3 measurements. UV absorption spectra obtained before and after the sample was used in the TR^3 measurements reveal no appreciable degradation during the Raman measurements. Acetonitrile Raman bands were used to calibrate all the Raman spectra with an estimated accuracy of ±5 cm^{-1} in absolute frequency.

The optimized geometry, frequency, and Raman activity of the vibrational mode for free MAP and H-bonded complexes containing one MAP and one or two H_2O molecules were obtained from B3LYP density functional theory (DFT) calculations employing a 6-311G** basis set and without any symmetry constraints. The calculations for the ground states were done using the closed shell formalism, while those for the triplet states were done using the open shell (UB3LYP) formalism. No imaginary frequency modes were observed at any of the optimized structures shown here. The spin density was obtained from the triplet calculation, and no appreciable spin contamination was found. For all the H-bonded complexes, the bonding energies required for the complex dissociating into free MAP and water molecule(s) were estimated based on the total energies (including zero point energy, ZPE) calculated for the corresponding species. All the calculations were done using the *Gaussian 98* program suite.[47]

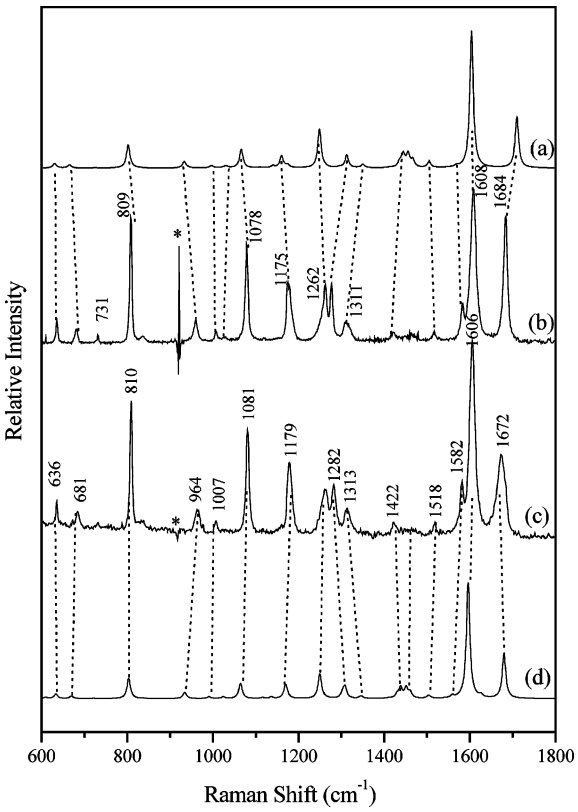

Figure 1. Comparison of the experimental normal Raman spectra of MAP obtained in MeCN (b) and 50% H_2O/50% MeCN (v:v) (c) with the DFT calculated spectra for the free ground state MAP (a) and the ground state of the carbonyl MAP−H_2O H-bond complex (d).

Results and Discussion

A. H-Bonding Effects on the Ground State MPA. Figure 1 b,c presents normal Raman spectra of MAP in neat MeCN and 50% H_2O/50% MeCN (by volume) mixed solvent, respectively. The spectrum in cyclohexane was not shown due to its similarity to those in these two solvents. The frequencies of the bands observed in the three solvents are listed in Table 1. It can be seen that most of the vibrational features show little sensitivity to a change in the solvent. However, the profile and frequency of some other vibrational features such as the characteristic carbonyl C═O stretching mode at around 1680 cm^{-1} displays remarkable sensitivity to the polarity and the H-bonding ability of the solvent. To make this clear, Figure 2 shows a comparison of the experimental and Lorentzian fitted C═O stretching bands in the three solvents. The C═O bands in cyclohexane and MeCN can be simulated adequately by a single Lorentzian band-shape with a similar bandwidth but a different frequency at 1695 cm^{-1} in cyclohexane and 1683 cm^{-1} in MeCN. The C═O band in the mixed solvent shows a significantly different feature: besides a further downshift in frequency, the band has a much broader bandwidth and an asymmetric profile. Obviously, this feature cannot be fitted by one Lorentzian; at least two Lorentzians are required to give a reasonable fit, and the result of such a fit is displayed in Figure 2c. The frequency of the underlying two subbands appears at 1681 and 1672 cm^{-1}, respectively, with the bandwidth (∼10 cm^{-1}) similar to those in MeCN and cyclohexane for the 1681

TABLE 1: Observed and Calculated Vibrational Frequencies (cm^{-1}) and Assignments for the Ground States of Free MAP and Carbonyl H-Bonded MAP−H_2O Complex

experimental			calculated		
normal Raman			frequency[a]		
MeCN	H_2O/MeCN	cyclohexane	MAP	MAP−H_2O	assignment description
636	636	636	631 (ν_{16})		CCC bending (ring)
681	685	677	665 (ν_{17})	670 (ν_{23})	C−C stretching (all, mainly C(9)−C(10)) + C(3/9)−O stretching
731	731		725 (ν_{18})	722 (ν_{24})	ring chair def.
809	810		802 (ν_{19})	804 (ν_{25})	C−C stretching (all) +O(7)−C(3>8) stretching
836	836		809 (ν_{20})	809 (ν_{26})	C−H bending (o.p., ring)
			831 (ν_{21})	837 (ν_{27})	C−H bending (o.p., ring)
959	964	955	933 (ν_{22})	934 (ν_{28})	C(9)−C(10) stretching + C(10)H3 wag
			943 (ν_{23})	940 (ν_{29})	C−H(18/19) bending (o.p.)
			971 (ν_{24})		C−H(20/21) bending (o.p.)
1007	1007		997 (ν_{25})	991 (ν_{30})	C−C stretching (ring)
			1021 (ν_{26})	1008 (ν_{31})	C−H16/17) twist + C(6)−C(9)−C(10) bending (o.p.)
			1030 (ν_{27})	1024 (ν_{32})	O(7)−C(8≫3) stretching
				1035 (ν_{33})	C(10)H3 twist + C−H(20>21) bending (o.p.)
1078	1081	1076	1066 (ν_{28})	1065 (ν_{34})	C−C stretching (all) + C(10)H3 wag
			1109 (ν_{29})	1116 (ν_{35})	C−H bending (i.p.)
			1140 (ν_{30})	1137 (ν_{36})	C−H(13/14) twist
1175	1179	1172	1160 (ν_{31})	1169 (ν_{37})	C−H bending (i.p., ring)
			1174 (ν_{32})	1172 (ν_{38})	C(8)H3 wag
			1249 (ν_{33})	1250 (ν_{39})	C−C stretching (all, major C(6)−C(9)) + O(7)−C(3/8) stretching
1261	1261		1261 (ν_{34})	1263 (ν_{40})	C−C stretching (all) + O(7)−C(3>8) stretching
	1282		1296 (ν_{35})	1303 (ν_{41})	C−H bending (i.p.)
1278			1313 (ν_{36})	1308 (ν_{42})	C−C stretching (mainly ring) + O(7)−C(3) stretching
1311	1313		1350 (ν_{37})	1346 (ν_{43})	C(10)H3 wag
			1414 (ν_{38})	1412 (ν_{44})	C−H bending (i.p.) + C−C stretching (ring)
			1435 (ν_{39})	1430 (ν_{45})	C(10)H3 deformation
				1438 (ν_{46})	C(8)H3 deformation + C(10)H3 deformation
				1438 (ν_{47})	C(8)H3 deformation + C(10)H3 deformation
			1441 (ν_{40})		C(8)H3 deformation
1421	1422		1445 (ν_{41})		C(10)H3 deformation
			1456 (ν_{42})	1451 (ν_{48})	C(8)H3 deformation
			1467 (ν_{43})	1460 (ν_{49})	C−H(13/14) deformation
1517	1518		1505 (ν_{44})	1504 (ν_{50})	C−C stretching (ring (19a)+ C(6)−C(9)) + C−H bending (i.p., ring) + C(3)−O stretching
1582	1582	1584	1568 (ν_{45})	1559 (ν_{51})	ring C−C stretching (ring)
1608	1606	1610	1604 (ν_{46})	1596 (ν_{52})	C−C stretching (ring + C(6)−C(9))
				1626 (ν_{53})	H_2O scissor
1684	1672	1695	1710 (ν_{47})	1680 (ν_{54})	C═O stretching

[a] Scaling factor for the calculated frequencies is 0.975 for free MAP and the MAP−H_2O complex.

cm^{-1} subband and a much broader bandwidth (~20 cm^{-1}) for the 1681 cm^{-1} subband.

Because of its sensitivity to solvent, the C═O stretching mode has been extensively used as a probe in spectroscopic studies of solute−solvent interactions.[31−34] The solvent dependence of the C═O frequency and band profile observed here are a typical reflection of the weak nonspecific electrostatic interaction and relatively strong specific solute−solvent-associated H-bonding interaction.[31−33,48] Solvent polarity and polarizability are the predominant solvent properties responsible for the nonspecific interaction. With an increasing solvent polarity, this interaction leads to a frequency downshift and modest bandwidth broadening for the C═O band. Depending on the extent of the solute−solvent H-bonding interaction and the aggregation character of the solvent medium, the specific interaction can cause a much more profound and complicated effect on the C═O mode than that of nonspecific interactions. Besides the excessive frequency downshift, a characteristic experimental indication for the specific interaction is the significant broadening of the C═O bandwidth caused by a decrease of the vibrational dephasing time.[49−52] Clearly, the observed C═O change on going from cyclohexane (a nonpolar solvent) to MeCN (a highly polar aprotic solvent) is due to the nonspecific interaction, and the broad low-frequency feature recorded in the water mixed solvent is from the H-bonded C═O group with the solvent water molecule(s). On the basis of the position and bandwidth, we attribute the higher frequency subband observed in the mixed solvent to the free C═O mode. The coexistence of the free and H-bonded C═O mode can be understood in terms of multiple H-bonding equilibria in the water mixed solvent system. This has been observed and studied before and was associated with the extensive aggregation nature of the water solvent system.[48,49] The predominant contribution of the H-bond C═O mode to the overall C═O band (Figure 2c) indicates that most of the ground state MAP exists with the their carbonyl group H-bonded with the surrounding water molecule(s). It is worthwhile to mention that the broad H-bond C═O band might possibly contain more than one band with each associated to a different H-bond configuration. According to the results of the DFT calculations, this band might be associated with the carbonyl H-bond complexes involving one and two water molecules, respectively.

Since the main interest of this paper concerns the specific H-bonding effect, the DFT calculations were done only to explore the structural and spectral changes caused by the H-bonding interaction by making a comparison between results computed for the free MAP and the various MAP−water H-bonded complexes. The optimized structure of the free MAP is displayed in Figure 3a, and its structural parameters are listed in Table 2. The MAP ground state was found to have a planar structure with all of the atoms (except the hydrogen atoms of the two methyl groups) in the same plane with the phenyl ring. The calculated Raman spectrum of the free MAP produced by

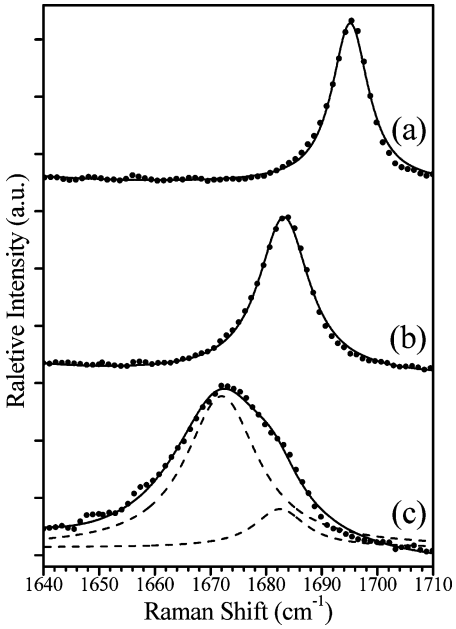

Figure 2. Comparison of the experimental C═O stretching Raman band obtained in cyclohexane (a), MeCN (b), and 50% H_2O/50% MeCN (v:v) solvents with 532 nm excitation.

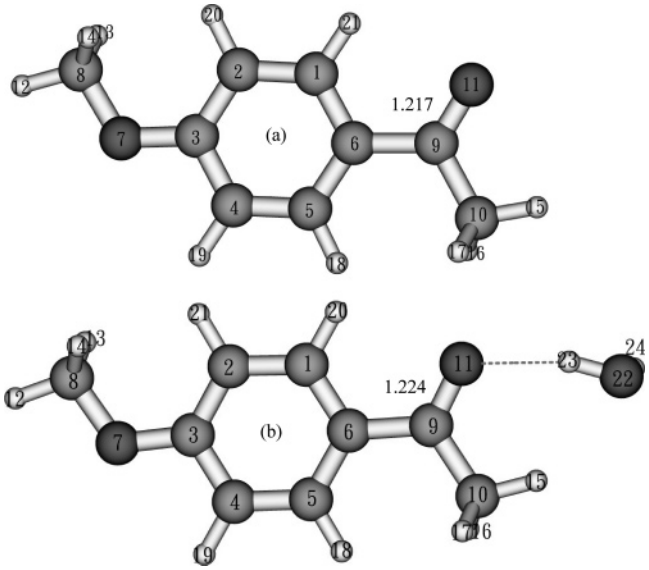

Figure 3. Optimized structure of the free ground state (a) and ground state of the carbonyl MAP−H_2O H-bond complex (b) calculated from the DFT calculation using the B3LYP method with a 6-311G** basis set. Bond lengths (in Å) are labeled for bonds showing significant change from free MAP to the H-bonded complex.

using a Lorentzian function with a 10 cm^{-1} bandwidth is presented in Figure 1a to compare directly with the experimental spectrum recorded in MeCN solvent. The reasonable agreement between calculated and experimental spectra allows a straightforward assignment of the experimental bands to the calculated vibrational modes. The calculated vibrational frequencies and the assignment descriptions including the predominant contribution to the vibrational modes are listed in Table 1 together with the experimental frequencies.

The calculations found that in addition to the structure with the methoxy C−O bond being *cis* to the *para* position carbonyl C═O bond (Figure 3), isomers with the C−O being *trans* to the C═O bond were also stable. The isomers with the C−O being *trans* to the C═O bond had a total energy slightly higher than that of the *cis* isomer by <0.3 kcal/mol, and the calculated Raman spectra are nearly identical for the two isomers. This indicates that the two conformations are nearly indistinguishable and can both contribute to the experimental observations. Similar results were also found for the triplet calculations as well as the calculations for the various ground and triplet state MAP−water H-bond complexes. To keep the discussion brief, we chose the *cis* conformation as an example here for the following discussion.

In addition to the H-bonding at the carbonyl oxygen (type A), MAP has two other active sites for the H-bonding interaction: the lone pair of methoxy oxygen (type B) and the π-aromatic ring (type C). DFT calculations with water molecule(s) put around the phenyl ring were found to result in separate MAP and H_2O molecules. This may indicate a weak nature for the H-bonding with the π-aromatic ring (type C) and is consistent with the experimental observation that the vibrational modes dominated by the ring motions are generally insensitive to the solvent H-bonding property (see Table 1 and Figure 1). Calculations on the H-bonded complexes of type A and B forms lead to stable structures with all positive vibrational frequencies. The optimized structure of MAP−H_2O (type A) is presented in Figure 3 and is compared to that of the free MAP. Computed structural parameters for this complex are listed in Table 2 together with those for the free MAP. The same information for MAP−H_2O (type B) and MAP−$2H_2O$ (type A) and MAP−$2H_2O$ (type A and type B) are given in the Supporting Information. The total energies (including ZPE) and the H-bond stabilization energies for the various H-bond complexes are also listed in the corresponding tables.

It can be seen that, within all of the H-bonded complexes, the structure of the MAP molecule is similar to that of free MAP with the H-bonds between the oxygen atoms and water hydrogen atoms lying approximately in the same plane as the MAP phenyl ring. The H-bond bond lengths are computed to be ∼2 Å for both the type A and B interactions. The H-bonds were found to lead to only local modifications to the MAP structure for both type A and type B interactions. Consequently, the structural changes caused by one type of the H-bonding have little influence for the H-bonding topology by the other type. The type A bonding leads to an increase in the C═O bond length by ∼0.01 Å and a slight shortening (by ∼0.005 Å) for the nearby C−C bonds (C6−C9 and C9−C10; see Figure 3 and Table 2). The type B interaction exclusively causes a lengthening of the C−O bond connecting the methoxy and the phenyl ring (by ∼0.01 Å; see Supporting Information). For both types of interactions, the structural parameters of the ring moiety remain almost unchanged.

From the calculated H-bond stabilization energy, the carbonyl located H-bond complexes (6.98 and 6.56 kcal/mol H-bond energy for the MAP−H_2O and the MAP−$2H_2O$ type A complex, respectively) are much more stable than the methoxy located complex (4.67 kcal/mol H-bond energy for MAP−H_2O type B complex). This implies that the H-bonding at the carbonyl moiety is more important than at the methoxy moiety in accounting for the experimental spectral differences observed in the neat MeCN and water mixed solvent systems. The calculated Raman spectra for the various H-bond complexes reflect the structural modification caused by the H-bond interactions. The localized and small extent of perturbation to the ground state structure caused by both A and B types of H-bonds suggests that the spectral variations that result from these H-bonds are also localized in nature. This is consistent with the observation that the major difference between the calculated spectra for the free MPA and the MAP−H_2O type

TABLE 2: Structural Parameters and Total Energies for the Ground States of Free MAP and Carbonyl H-Bonded MAP−H_2O Complex Calculated from DFT Calculations Using the B3LYP Method with 6-311G Basis Set**

bond lengths (Å)			bond angles (deg)			dihedral angles (deg)		
	MAP	MAP −H_2O		MAP	MAP−H_2O		MAP	MAP−H_2O
C1−C2	1.389	1.388	C1−C2−C3	119.5	119.8	C1−C2−C3−C4	0	−0.1
C2−C3	1.401	1.401	C2−C3−C4	119.6	119.6	C1−C2−C3−O7	180	179.9
C3−C4	1.402	1.403	C3−C4−C5	120.1	120.1	C2−C3−O7−C8	0.0	−0.3
C4−C5	1.384	1.382	C4−C5−C6	121.0	121.1	C4−C5−C6−C9	180.0	179.8
C5−C6	1.405	1.407	C5−C6−C1	118.2	118.2	C5−C6−C9−C10	0.0	0.9
C6−C1	1.399	1.402	C6−C1−C2	121.5	121.2	C1−C6−C9−O11	0.0	0.7
C6−C9	1.494	1.486	C6−C9−C10	118.7	119.0	C6−C9−C10−H15	180.0	179.2
C9−C10	1.520	1.519	C6−C9═O11	121.0	121.9	C6−C9−C10−H16	59.7	58.8
C3−O7	1.357	1.355	C2−C3−O7	124.7	124.7	C6−C9−C10−H17	−59.7	−60.7
C8−O7	1.423	1.425	C3−O7−C8	118.8	118.8	C6−C9−O11−H23		3.9
C9═O11	1.217	1.224	C5−C6−C9	123.3	122.3	C9═O11−H23−O22		−46.6
O11−H23		1.944	C9═O11−H23		139.0	O11−H23−O22−H24		−53.2
H23−O22		0.970	O11−H23−O22		162.4			
O22−H24		0.962	H23−O22−H24		103.0			

[a] Total energy (hartrees): MAP, −499.3817; MAP−H_2O, −575.8190. [a] H-bond energy (kcal/mol): 6.9784.
[a] Including ZPE.

A complex is the frequency shift of the carbonyl C═O stretching mode. On the other hand, because of the absence of a particular mode dominated by the stretching vibration of the $C_{ring}-O_{methoxy}$ bond, the computed spectrum for the MAP−H_2O type B complex is rather similar to that of the free MAP calculated spectrum. We therefore conclude that the spectral differences observed in the neat solvent (cyclohexane and MeCN) versus the 50% H_2O/50% MeCN mixed solvent are relevant primarily to the carbonyl H-bond interactions. Although the methoxy H-bond strength is weaker than the carbonyl H-bond strength, we cannot rule out the possibility for the existence of this type of H-bond due to the lack of vibrational features that can easily probe it.

All the calculated spectra for the H-bond complexes containing the type A interaction (MAP−H_2O type A, MAP−$2H_2O$ type A, and MAP−$2H_2O$ types A and B) are generally similar to one another except for small differences in the carbonyl C═O stretching frequencies. On the basis of this and the most stable H-bond configuration for the MAP−H_2O (type A) complex and to simplify the following discussion, only the calculated spectrum for this complex is presented in Figure 1 (as spectrum d) to compare with the experimental spectrum recorded in the water mixed solvent. Calculated spectra for the other complexes are given in the Supporting Information. The calculated frequencies of the carbonyl located MAP−H_2O complex are listed in Table 1 together with the experimental frequencies and those computed for the free MAP. It can be seen that the general spectral profile of the H-bond complex is similar to that for the free MAP (Figure 1a), but the frequency shifts are obvious for the particular modes relevant to the H-bonding interaction. The carbonyl C═O stretching motion was calculated to shift down by ∼28 cm^{-1} from the free to the H-bond complex, reproducing the experimental observation of a 23 cm^{-1} C═O downshift on going from MAP in cyclohexane to the water mixed acetonitrile solvent. Other small shifts, like the upshift of the ∼960 cm^{-1} experimental band, are also reproduced by the calculation: the 9 cm^{-1} upshift observed upon going from the cyclohexane to water mixed solvent agrees reasonably well with the calculated shift of 12 cm^{-1}. This mode has a large contribution from the C9−C10 stretching motion (see Figure 3 and Table 2), and the upshift is due to a shortening of this bond caused by the carbonyl located H-bond.

It is interesting to mention the calculated result that, for the carbonyl located H-bond, the average H-bond energy for the complex containing two water molecules (see Supporting Information) is only slightly smaller than that for the complex involving one water molecule. This implies that the existence of one H-bonded water molecule has little influence on the capacity of the carbonyl group to H-bond with another water molecule. This means further that the complexes with both one and two waters H-bonded to the carbonyl oxygen could account to a similar degree for the C═O spectral difference observed in the water mixed solvent versus neat MeCN. Since the calculation shows additional weakening of the C═O bond (although only slightly, see Table 2 and Table 1S in Supporting Information) and some extra downshift of the C═O stretching frequency (calculated ∼28 cm^{-1}) upon H-bonding with the second water molecule, the involvement of these two kinds of H-bond complexes might account for the extraordinary broadness of the H-bonded C═O band profile recorded in the mixed solvent system.

B. Time-Resolved Resonance Raman Spectra of the Free and H-Bonded Triplets of MAP. In the TR^3 measurements, the 267 nm pump wavelength lies in the lowest allowed $\pi\pi^*$ (S_3) absorption band (with a maximum around 267 nm), and the 400 nm (ps-TR^3) and 416 nm (ns-TR^3) probe wavelengths are within the strong T_1-T_n absorption band reported previously.[4a,15] Figures 4 and 5 display representative ps-TR^3 (a) and ns-TR^3 (b) spectra of MAP in neat acetonitrile and 50% H_2O/50% MeCN mixed solvents, respectively. The corresponding picosecond and nanosecond TR^3 spectra measured in cyclohexane were found to be similar to those recorded in neat MeCN. This is consistent with a previous transient absorption study on the MAP triplet in the two solvents.[15] From Figures 4 and 5, one can see that, in both neat MeCN and water mixed solvent, the same spectral features were observed in the late picosecond spectra (with a delay time after 20 ps) and the corresponding nanosecond spectra, indicating that the same species is detected in both cases. Because of the better spectral resolution of the nanosecond than picosecond TR^3 measurement, the ns-TR^3 spectra are much better resolved than the corresponding ps-TR^3 spectra. The very broad and severely overlapped ps-TR^3 feature at ∼1400 cm^{-1} in the mixed solvent is resolved clearly into seven bands in the ns-TR^3 spectra (see Figure 5).

From Figures 4 and 5, it can be seen that the initial picosecond spectrum (the 0, 2, and 5 ps spectrum) is almost featureless, but they evolve rapidly at very early times and decay in intensity on the nanosecond time scale. By fitting the Raman features with Lorentzian band shapes, Figures 6 and 7 display the

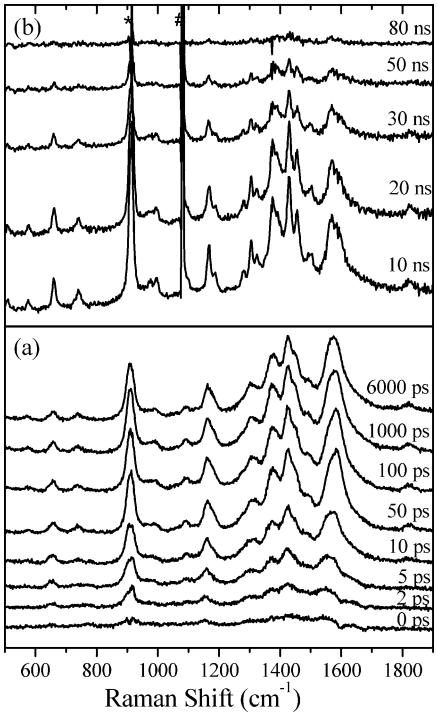

Figure 4. Picosecond (a) and nanosecond (b) time-resolved resonance Raman spectra of MAP in MeCN obtained with 266 nm pump excitation wavelength and 400 nm (ps) and 416 nm (ns) probe wavelengths at various delay times that are indicated next to the spectra. The asterisks (*) mark solvent subtraction artifacts. The # is due to a stray laser line.

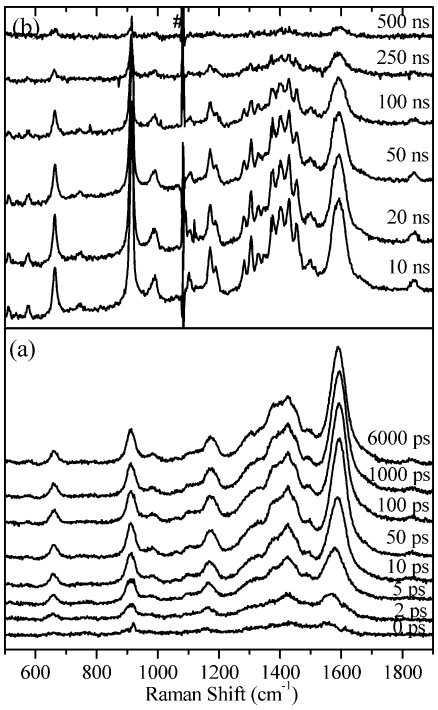

Figure 5. Picosecond (a) and nanosecond (b) time-resolved resonance Raman spectra of MAP in 50% H_2O/50% MeCN (v:v) obtained with 266 nm pump excitation wavelength and 400 nm (ps) and 416 nm (ns) probe wavelengths at various delay times that are indicated next to the spectra. The # is due to a stray laser line.

dynamics of the early time formation and later time decay of the species observed in the neat and water mixed MeCN solvents, respectively. As shown together with the experimental data points, the kinetics can be fit well by using a one exponential growth and decay function for both picosecond and

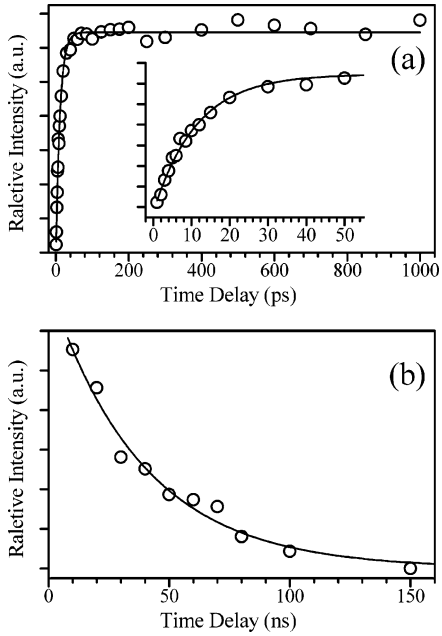

Figure 6. Time dependence of the ~660 cm^{-1} band area obtained in the picosecond (a) and nanosecond (b) time-resolved resonance Raman spectra of MAP in MeCN displayed in Figure 4. The insert in panel (a) shows the early picosecond dynamics of the ps-TR^3 spectra.

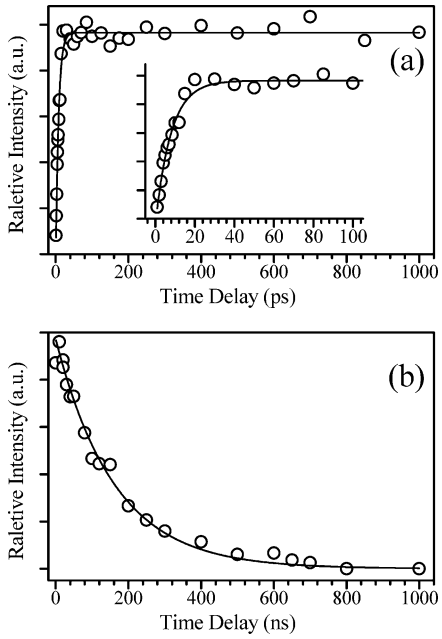

Figure 7. Time dependence of the ~660 cm^{-1} band area obtained in the picosecond (a) and nanosecond (b) time-resolved resonance Raman spectra of MAP in 50% H_2O/50% MeCN (v:v) displayed in Figure 5. The insert in panel (a) shows the early picosecond dynamics of the ps-TR^3 spectra.

nanosecond data in the two solvents. Time constants of ~8 and 11 ps were found for the early time growth and ~40 and 160 ns (open air experimental condition) for the nanosecond decay in the neat and mixed MeCN solvents, respectively. Nanosecond TR^3 measurements performed under open air, N_2, and O_2 purged conditions indicate that the nanosecond decay component is sensitive to the presence of oxygen. With an increasing amount of oxygen introduced into the sample system, the decay times decrease dramatically. This provides further support along with the choice of probe wavelength to detect selectively the T_1-T_n transition and leads us to attribute the TR^3 spectra observed in the two solvents to a species that is triplet in nature. It is,

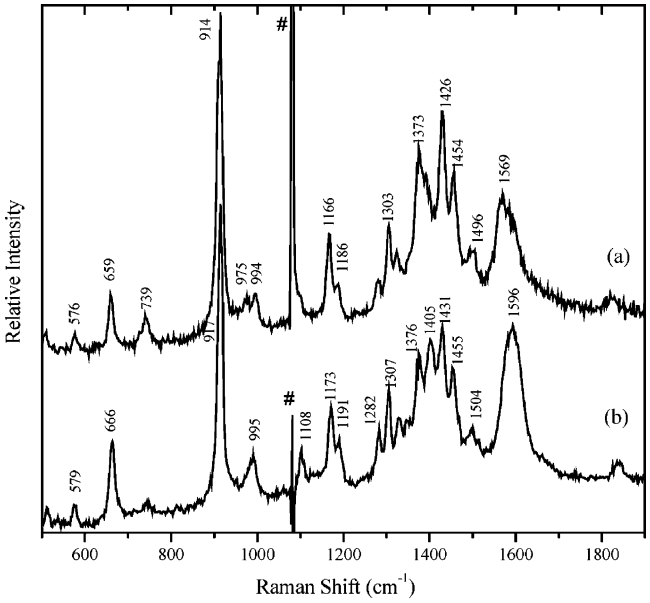

Figure 8. Comparison of the nanosecond time-resolved resonance Raman spectra of MAP obtained in MeCN (a) and 50% H_2O/50% MeCN (v:v) (b) with 267 nm pump excitation and 416 nm probe excitation at a time delay of 10 ns.

however, significant that the lifetime of the species observed in the water mixed solvent (160 ns) is 4 times longer than that in the neat MeCN (40 ns) solvent. In addition, by comparing carefully the ns-TR[3] spectra recorded in the two solvents (see Figure 8), one can find many subtle but definite differences: the frequencies of many features show an upshift on going from the neat MeCN solvent to the water mixed MeCN solvent, and there are obvious divergences in the spectral appearance, especially in 1200−1500 cm^{-1} region in the mixed water/MeCN solvent as compared to the neat MeCN solvent. This is obvious evidence that the spectra recorded in the two solvents are from two distinct species. On the basis of the ground-state H-bond behavior combined with a general knowledge of the increased basicity of the carbonyl oxygen for the AC $\pi\pi^*$ triplet state,[20−26,53,54] we attribute these spectral changes in the two solvent systems to be due to the triplet of free MAP and water H-bonded MAP, respectively, in the neat and mixed solvent. As discussed next, the triplet DFT calculations provide theoretical evidence to support such an assignment.

The rapid formation of the triplets in the two solvents indicates that there is rapid ISC conversion for both free and H-bond complex species. This is analogous to the triplet formation dynamics we observed recently for closely related compound *p*-hydroxyacetophenone and two of its derivatives.[9,10] A similar fs-TRF measurement for MAP showed its fluorescence decays with time constant of ∼2 ps in both neat MeCN and 50% H_2O/50% MeCN solvent. This corresponds to an ISC rate of $\sim 5 \times 10^{11}$ s^{-1}. Such a quick ISC conversion is consistent with the unity triplet quantum yield reported previously for MAP in the solution phase.[16] The slightly longer time scale observed here for the early picosecond triplet spectral evolution (with 8 and 11 ps time constants in the neat and mixed MeCN, respectively) than the ∼2 ps ISC conversion from the fs-TRF measurement is likely due to the combined consequences of the triplet formation and the relaxation of the excess energy of the initially formed energetic triplet state produced from the rapid ISC conversion. Characteristic evidences for the excess energy relaxation are the early time bandwidth narrowing and frequency upshift of the picosecond Raman features (see Figures 4a and 5a) and that the temporal changes of this bandwidth and frequency are found to occur with similar time constants to the intensity build-up of the triplet TR[3] features.[10,55−59] The triplet energy of MAP in the solution phase was determined to be ∼25 000 cm^{-1}.[13] Since ISC is the predominant way to dissipate the excitation energy absorbed by the singlet excited state, the 267 nm pump pulse used here can introduce a great amount of excess energy (∼12000 cm^{-1}) into the initially generated triplet. Relaxation of such a large amount of energy on the triplet manifold is therefore expected, and this has been suggested to occur for a few of other AC compounds.[60−62]

As illustrated previously, most ground state MAP molecules in the 50% H_2O/50% MeCN solvent are H-bonded at the carbonyl site with the surrounding water molecules, and they can be described as H-bonded complexes. Since the UV spectrum of MAP in 50% H_2O/50%,MeCN shows only a slight red-shift (with the maximum at ∼272 nm) from that in neat MeCN (with the maximum at ∼267 nm), the 267 nm photoexcitation of the complex(es) leads to, like that for free MAP in MeCN, instant formation of the S_3 singlet state upon which the fluorescence back to ground state, IC to lower singlet (including ground state), and ISC to triplet can occur. Our recent fs-KTRF study found that for a similar compound, the depopulation of the S_3 singlet and ISC to triplet proceeds following the S_3 ($\pi\pi^*$) → S_1 ($n\pi^*$) → T_1 ($\pi\pi^*$) sequence and that the dynamics of this process is rather the same in both the neat and the water mixed solvent.[9] Our results show that similar time constants observed for the development of the triplet Raman spectra in the two solvents are consistent with this and indicates that the presence of the H-bonding interactions does not influence the dynamics of energy dissipation and ISC conversion for this particular AC compound. This can be understood in terms of the same relative energy order of the MAP $n\pi^*$ and $\pi\pi^*$ excited states in the two solvents, although the carbonyl H-bond can cause a slight decrease of the $n\pi^*$ and $\pi\pi^*$ single gap and an increase of the $n\pi^*$ and $\pi\pi^*$ triple gap.[13−19]

It is well-known that an existing H-bond constantly breaks and reforms.[48,49] However, it was found in several previous time-resolved studies[11,50] that the time scale for the molecule to develop a new H-bond with solvent molecule(s) is much slower and occurs at the tens of picosecond time scale. On the basis of this and the rapid ISC rate in the water mixed solvent, we infer that the H-bond configurations for the triplet H-bond complexes are just the modified (strengthened or weakened) counterparts of that for the ground state H-bond complexes, or in an other words, there is no new H-bond interaction formed on the triplet manifold. This is corroborated with the calculated structures showing that the H-bond conformations for the triplet complexes are not very different from their ground state counterparts (section D). This is along with the femtosecond work reported by Nibbering and co-workers showing that reorganization of the H-bond configuration caused by the electronic excitation occurs on the hundreds of femtosecond time scale.[36] In this connection, we can describe generation of the triplet H-bonded complexes as:

$$S_0\,[\text{MAP}-\text{water}]_{\text{complex}} \xrightarrow{h\nu} S_3\,[\text{MAP}-\text{water}]_{\text{complex}} \xrightarrow{\text{IC}} S_1\,[\text{MAP}-\text{water}]_{\text{complex}} \xrightarrow{\text{ISC}} T_1[\text{MAP}-\text{water}]_{\text{complex}}$$

C. Structure of Free MAP Triplet State. The calculated geometry and relevant structural parameters for the triplet of the free MAP are given in Figure 9 and Table 3, respectively. A triplet energy of 69.0 kcal/mol can be estimated based on the calculated total energies for the triplet (listed in Table 3) and the ground state (Table 2). This triplet energy is in good

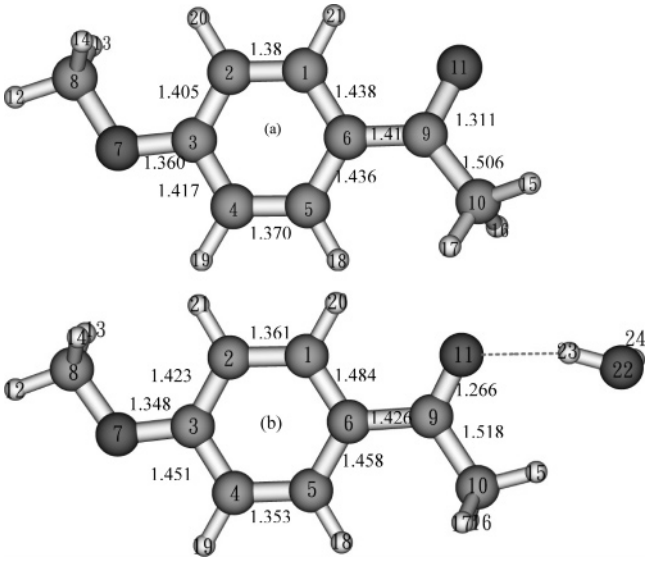

Figure 9. Optimized structure of the free triplet state (a) and triplet of carbonyl MAP−H_2O H-bond complex (b) calculated from the DFT calculation using the UB3LYP method with a 6-311G** basis set. Bond lengths (in Å) are labeled for bonds showing significant change from free MAP triplet to the triplet H-bonded complex.

agreement with the ∼70 kcal/mol experimental value reported from phosphorescence measurements.[3d,13] Figure 10 a,b displays a comparison between calculated and experimental (the 10 ns spectrum shown in Figure 4) triplet spectra, respectively. It can be seen that the calculation reproduces reasonably well the experimental spectrum, indicating that the optimized geometry is reasonable. The differences in the relative intensities among the various features between experimental and calculated spectra are within the expectations since the former is obtained with resonance enhancement while the latter corresponds to a normal Raman spectrum for the triplet. Preliminary assignments have been made straightforwardly based on the correlation between the two spectra. The observed triplet band frequencies together with the corresponding computed values and their tentative assignments are summarized in Table 4. To help identify the triplet carbonyl C═O stretching mode, a frequency calculation on the carbonyl isotopic substituted MAP−^{13}C and MAP−^{18}O have been performed, and these results are also given in Table 4.

Comparison of the structural parameters calculated for the free triplet (Table 3) and the ground state (Table 2) indicates that there are substantial geometry changes in the triplet state. On going from the ground to the triplet state, the carbonyl C═O bond length increases remarkably by ∼0.1 Å and appears to be more like a single bond as indicated by its similarity to the bond length of the single C−O bond connecting the ring and the methoxy moiety. The length of the C−C bond joining the ring and carbonyl moiety decreases substantially by ∼0.08 Å, implying an increased extent of conjugation between the ring π system and the carbonyl π electrons. There are modest decreases for the bond lengths of the ring center C−C bonds but an increase for ring shoulder C−C bonds. These changes in the ring C−C bond lengths means that there is an increasing amount of quinoidal character for the triplet as compared to the ground state, and this is in agreement with the general $\pi\pi^*$ nature of the MAP triplet. It is, however, important to mention that the triplet $\pi \rightarrow \pi^*$ transition, rather than being localized on the ring moiety, leads to a delocalized change of the π electrons within both the ring and the carbonyl subgroups. The latter is reflected by the substantial lengthening of the carbonyl C═O bond in the triplet as compared to the ground state. The same triplet configuration has been observed for the related compound HA and its derivatives.[10]

Additional conformational changes in the triplet involve the variation of the relative orientations between the ring and the carbonyl connected groups. Unlike the planarity of the ground state, the plane constituted by the carbonyl and the nearby -CH_3 group carbon atom twists out of the ring plane by ∼16°, and the -CH_3 group rotates around the C9−C10 bond by ∼30° in the triplet state. We note that the same type of orientation change (between the ring and the carbonyl related groups) has been proposed for several AC compounds (including the MAP triplet studied here[63]) previously by using singlet−triplet state absorption and phosphorescence measurements.[64−66] The changes have been associated with the vibrational coupling between the close-lying $n\pi^*$ and $\pi\pi^*$ triplet states.[13] The torsional vibration of -C(O)CH_3 with respect to the ring and the rotation of the -CH_3 group have been identified as effective out-of-plane modes to couple the two triplets, and the coupling was suggested to lead to a conformational change along the two coordinates for the triplet structure.[63] This orientation variation has been considered an important factor in influencing the triplet reactivity and dynamics of the triplet depopulation.[63,67]

From Table 4 and by the comparison between the experimental (Figure 4b) and calculated (Figure 4a) triplet spectrum, one can see that most of the observed bands are from the vibrations of various ring modes (mainly the ring C−C stretching motions). It is, however, significant that there is no mode found to be from the carbonyl C═O stretching or with a major contribution from this vibrational motion. This is manifested by the calculated frequency shifts on going from the normal MAP to carbonyl ^{13}C and ^{18}O substituted MAP. As shown in Table 3, there are three experimental features 1373, 1186, and 1166 cm^{-1} in 1000−1800 cm^{-1} frequency range computed to be frequency sensitive to the carbonyl ^{13}C and ^{18}O substitutions. Among the three modes, only the 1186 cm^{-1} feature displays a frequency downshift upon both ^{13}C and ^{18}O substitution, while the other two are sensitive only to the ^{13}C substitution. This indicates that the former contains contributions from the C═O stretching, while the latter are mainly from the vibrations containing the carbonyl carbon atom (see Table 3). However, even for the 1186 cm^{-1} feature, the extent of the shifts, calculated to be 11 and 6 cm^{-1} upon the ^{13}C and ^{18}O, respectively, are far less than those observed for the normal localized C═O stretching mode (15 and 24 cm^{-1} upon the ^{13}C and ^{18}O, respectively).[69] This indicates even the 1186 cm^{-1} feature has only partial contribution from the C═O stretching motion to this feature. The absence of a localized triplet C═O stretching mode has been reported in several early publications for AC compounds with a flexible carbonyl group and has been interpreted to be due to the extensive mixing of this mode with other vibrations with similar frequencies so that it does not exist as a separate normal mode as that in the ground state.[65,68−70] The small isotopic shifts observed here are in agreement with this and imply that a similar situation occurs for the MAP $\pi\pi^*$ triplet.

We note, however, that our view on the triplet C═O stretching vibration appears somewhat different from a time-resolved infrared (TRIR) result reported by Srivastava and co-workers.[14] The frequencies of the IR bands are given in Table 3 so as to compare them with the Raman bands obtained in this work. In the TRIR work, a 1462 cm^{-1} transient IR feature has been associated with the triplet C═O stretching vibration based on its frequency sensitivity to the carbonyl ^{13}C isotopic substitution.

TABLE 3: Structural Parameters and Total Energies for Triplet State of Free MAP and Carbonyl H-Bonded MAP−H_2O Complex Calculated from DFT Calculations Using the UB3LYP Method with 6-311G Basis Set**

bond lengths (Å)			bond angles (deg)			dihedral angles (deg)		
	MAP	MAP−H_2 O		MAP	MAP−H_2O		MAP	MAP−H_2 O
C1−C2	1.38	1.361	C1−C2−C3	120.2	120.4	C1−C2−C3−C4	−0.5	0.5
C2−C3	1.405	1.423	C2−C3−C4	119.3	119.6	C1−C2−C3−O7	179.1	−179.8
C3−C4	1.417	1.451	C3−C4−C5	121.0	121.0	C2−C3−O7−C8	2.3	0.4
C4−C5	1.370	1.353	C4−C5−C6	120.9	120.8	C4−C5−C6−C9	−179.9	−178.6
C5−C6	1.436	1.458	C5−C6−C1	117.0	117.0	C5-−C6−C9−C10	−9.5	−0.2
C6−C1	1.438	1.484	C6−C1−C2	121.5	121.0	C1−C6−C9−O11	−16.5	0.0
C6−C9	1.414	1.426	C6−C9−C10	125.8	120.5	C6−C9−C10−H15	−151.1	179.9
C9−C10	1.506	1.518	C6−C9═O11	117.0	120.5	C6−C9−C10−H16	89.8	60.3
C3−O7	1.360	1.348	C2−C3−O7	125.3	126.0	C6−C9−C10−H17	−31.7	−60.4
C8−O7	1.422	1.429	C3−O7−C8	118.7	119.3	C6−C9−O11−H23		−6.8
C9═O11	1.311	1.266	C5−C6−C9	122.8	123.0	C9═O11−H23−O22		56.3
O11−H23		1.897	C9═O11−H23		140.1	O11−H23−O22−H24		47.3
H23−O22		0.973	O11−H23−O22		162.8			
O22−H24		0.962	H23−O22−H24		102.7			

[a] Total energy (hartrees): MAP, −499.2725; MAP−H_2O, −575.7111. [a] H-bond energy (kcal/mol): 7.8425.
[a] Including ZPE.

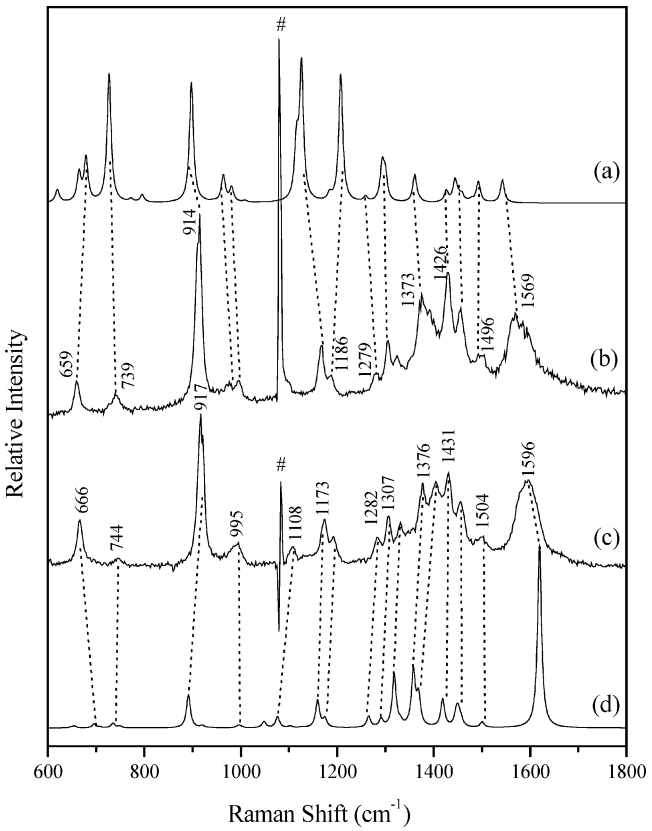

Figure 10. Comparison of the experimental resonance Raman spectra of MAP obtained in MeCN (b) and 50% H_2O/50% MeCN (v:v) (c) with the DFT calculated spectra for the free triplet of MAP (a) and triplet of the carbonyl MAP−H_2O H-bond complex (d).

This assignment may be inconclusive because the feature is not sensitive to the carbonyl ^{18}O substitution.[14] According to our DFT results, this IR feature might correspond to the 1450 cm^{-1} computed feature (Table 3), which has contributions from the $C_{ring}-C_{carbonyl}$ stretching and methyl deformation motions.

As compared with the typical double-bond character of the ground state carbonyl configuration, the single-bond nature of the triplet carbonyl implies a remarkable reduction of the carbonyl bond order in the MAP triplet. This originates from a change of electronic structure caused by the $\pi\pi^*$ transition. The calculations show that both the bonding and the antibonding π orbital have contributions from the ring π electrons and the carbonyl π electrons with the bonding orbital residing more on the ring and antibonding more on the carbonyl orbital. The $\pi\pi^*$ transition associated with such a molecular orbital change leads to an increased electron density on the carbonyl antibonding orbital that results in substantial weakening of the carbonyl bond strength as shown by the increase of the C═O bond length in the triplet state as compared with the ground state. At the same time, this increases the H-bond accepting ability for the carbonyl oxygen. Although the increase of the carbonyl oxygen basicity in the $\pi\pi^*$ triplet state has been considered to be a general phenomena for AC compounds in previous studies,[20−26,53,54] the results here for MAP using TR^3 spectroscopy and a direct structural study of the configuration of the triplet H-bond complexes represent to the best of our knowledge one of the first vibrational investigations of this kind of water H-bonded complexes of these compounds.

D. Structure of the Triplet MAP−Water H-Bond Complexes. The calculated geometry and relevant structural parameters for the triplet state of the MAP−H_2O complex with the type A H-bond are presented together with the data for the free triplet state in Figure 9 and Table 3, respectively. Corresponding results for the triplet complexes of MAP−$2H_2O$ (type A), MAP−H_2O (type B), and MAP−$2H_2O$ (type A and B) are given in the Supporting Information. As compared with the free MAP triplet state, the stabilization energy for the triplet H-bond complexes (Table 3 and Table 2S in Supporting Information) were estimated to be 7.84 and 4.63 kcal/mol, respectively, for types A and B MAP−H_2O complexes, respectively. As compared with the corresponding ground state H-bond energy, this implies that the type A H-bond is strengthened substantially, while the type B H-bond is weakened in their triplet state as compared with their respective ground state. The weakness of the type B H-bond is manifested also in the results for the optimized structure and calculated Raman spectra (see Figure 10 and the Supporting Information). For example, one can find from the optimized geometry data that including the type B H-bond leads to only a small geometric modification such that the structures and the corresponding spectra are similar for the configurations with and without the type B H-bond. The carbonyl type A H-bond, on the other hand, results in extensive structural variation and was found to be the major cause for the TR^3 spectral difference observed in the water mixed and neat MeCN solvents. We have also considered the possibility that the water might form H-bond with the ring moiety for the MAP triplet, but the calculations failed to locate any stable

TABLE 4: Observed and Calculated Vibrational Frequencies (cm^{-1}) and Tentative Assignments for Free MAP Triplet State

		calculated				
			frequency[a]			
experimental	IR[b]		normal	^{13}C	^{18}O	assignment description
576		ν_{16}	620	619	619	CCC bending
		ν_{17}	665	663	662	C−C stretching (all) + O(7)−C(3>8) stretching
659		ν_{18}	679	679	678	ring chair def. (4) + C−C stretching (all) + C−O stretching + C═O stretching
739		ν_{19}	727	726	727	C−C stretching (all) + C−O stretching
		ν_{20}	772	772	772	ring C−C o.p. deformation (17b) + C−H bending (o.p., ring)
		ν_{21}	795	795	795	C−H bending (o.p., ring)
914		ν_{22}	898	894	891	C−C stretching (all) + O(7)−C(3>8) stretching + C═O stretching
		ν_{23}	923	923	923	C−H(20/21) bending (o.p.)
		ν_{24}	943	943	942	C−H(18/19) bending (o.p.)
975		ν_{25}	964	963	959	C(10)H3 wag
994		ν_{26}	981	980	981	C−C stretching (ring)
		ν_{27}	1008	1005	1008	C(10)H3 wag
		ν_{28}	1041	1040	1041	C(8)−O(7) stretching
1166		ν_{29}	1116	1105	1113	C−H bending (i.p., ring) + C−C stretching (mainly C(6)−C(9))
		ν_{30}	1126	1120	1125	C−C stretching (ring + C(9)−C(10)) + C−H(18/19) bending (i.p.)
		ν_{31}	1150	1150	1150	C−H(13/14) twist
		ν_{32}	1184	1184	1184	mainly C(8)H3 wag
1186		ν_{33}	1207	1196	1201	C(9) −C(10) stretching + C═O stretching + C−H bending (i.p., ring)
1279	1284	ν_{34}	1259	1258	1258	C(3/8) −O stretching + C−C stretching (ring) + C−H bending (i.p., ring)
1303		ν_{35}	1293	1292	1293	C−C stretching (mainly ring) + C−H bending (i.p., ring)
1322	1332	ν_{36}	1300	1299	1300	C−C stretching (ring) + O(7)−C(3≫8) stretching + C−H bending (i.p., ring)
1373	1378	ν_{37}	1361	1340	1360	C−C stretching (all, mainly C(6)−C(9)) + C═O stretching
		ν_{38}	1371	1371	1371	C(10)H3 wag
1426	1430	ν_{39}	1426	1426	1426	C−C stretching (ring) + C−H(19/20) bending (i.p.)
1454		ν_{40}	1444	1444	1444	mainly C−H(16/17) scissor
	1462	ν_{41}	1450	1450	1450	mainly C(8) H3 deformation + C6−C9 stretching
		ν_{42}	1458	1458	1458	mainly C(8) H3 deformation + C−H(15/18) scissor
		ν_{43}	1469	1469	1469	C(8)H3 deformation
		ν_{44}	1478	1477	1478	mainly C(13/14) scissor
		ν_{45}	1489	1485	1488	C−C stretching (all) + C═O stretching + C(8/10)H3 deformation
1496		ν_{46}	1493	1492	1493	C−C stretching (all)
1569		ν_{47}	1543	1541	1542	C−C stretching (all) + O(7)−C(3) stretching
1820						2 ν_{22} (914)

[a] Scaling factor for the calculated frequencies is 0.986. [b] From ref 14. i.p.: in-plane; o.p.: out-of-plane.

structure. We therefore conclude that the type B as well as the ring H-bond plays only a minor role for the MAP triplet H-bond interaction.

The calculations also show that, like the case for the ground state, the carbonyl located triplet complex involving one water molecule is slightly more stabilized than the one containing two water molecules. From the experimental viewpoint, the single-exponential decay for the lifetime of the triplet complex and the well-resolved appearance for all of the features in the ns-TR^3 spectra recorded in the water mixed solvent suggests that (i) there is no dissociation of the triplet H-bond complex back to the free triplet within the triplet lifetime and (ii) there is only one species that is responsible for the experimental observation. Point (i) is consistent with the strong nature of the triplet carbonyl H-bond interaction. Point (ii) combined with the calculation results leads us to conclude that the carbonyl located H-bond complex containing one water molecule is the triplet species that mostly accounts for the TR^3 observation in the mixed water/MeCN solvent.

From Tables 2 and 3 and Figures 3 and 9, one can find that the geometry of the carbonyl H-bonded triplet complex is significantly different from that of the free triplet state in terms of the bond lengths of the ring and the -C(O)CH_3 moieties and the relative orientation between the two subgroups. First of all, the carbonyl C═O bond length is shorter in the H-bond complex (1.27 Å) than the free MAP triplet (1.31 Å). With reference to the ground state carbonyl band lengths (1.22 and 1.23 Å for the free and carbonyl H-bond complex, respectively), this implies some carbon double bond character for the carbonyl group for the triplet complex. This is significant since the H-bond leads generally to an increase of the bond length of the H-bond acceptor group,[11,31−34,50] like what we observed in the ground state MAP H-bond complexes. The shortening of the carbonyl bond length in the complex as compared to the free triplet state implies that the triplet carbonyl H-bond is not a localized weak perturbation and that it is strong in nature. This results in a significant modification to the overall triplet configuration, and this is indicated by the other structural and electronic property differences calculated between the triplet state complex and the free triplet state.

For example, due to the further shortening (by ∼0.02 Å) and lengthening (by ∼0.02−0.05 Å) of the ring center C−C and shoulder C−C bond lengths, respectively, the ring becomes obviously more quinoidal in character for the triplet state complex than the free MAP. The length of the C−C bond joining the ring and the carbonyl lengthens a bit more (by ∼0.02 Å) in the triplet state complex than in the free MAP. This implies there is a lesser extent of conjugation between the ring and carbonyl π systems for the triplet state complex than that in the free triplet state. In addition, unlike the twisted -C(O)CH_3 orientation with respect to the ring plane in the free MAP triplet state, the triplet state complex is planar in geometry, like that in the ground state. The planar H-bonding configuration of the donor H_2O molecule to the acceptor MAP is quite similar in the triplet complex to that in the counterpart ground state complex, but the H-bond bond length (O11−H23) is about 0.04 Å shorter in the triplet than that in the ground state. This corroborates the result of the computed H-bond stabilization energies and indicates the stronger H-bond strength in the triplet complex than its ground state counterpart.

TABLE 5: Spin Density Distributions for the Triplet States of the Free MAP and Carbonyl MAP−H_2O H-Bond Complex Obtained from DFT UB3LYP/6-311G Calculation**

	MAP	MAP−H_2O
ρC_1	0.278	0.336
ρC_2	−0.124	−0.109
ρC_3	0.286	0.494
ρC_4	−0.048	0.142
ρC_5	0.168	0.038
ρC_6	0.085	0.538
ρO_7	0.073	0.155
ρC_8	−0.007	−0.014
ρC_9	0.394	0.064
ρC_{10}	0.005	−0.012
ρO_{11}	0.846	0.365
ρO_{12}		0.000

From the geometry differences between the free triplet state and the H-bond triplet state complex and their comparison with the corresponding ground state structures, it is clear that on going from the ground state to the triplet state, the structural alternation appears more confined to the phenyl ring moiety for the H-bond complexes than for the free MAP. As discussed previously, the triplet H-bond complex originates dynamically from the corresponding ground state counterparts. It is thus reasonable to infer that it is the carbonyl H-bond that leads to the $\pi\pi^*$ conjugation being more localized in the ring subgroup for the triplet carbonyl complex than for the free MAP triplet state.

The ring locating $\pi\pi^*$ nature of the complex triplet state is illustrated also by a comparison of the calculated triplet state free spin density results (listed in Table 5) for the free MAP triplet state and the triplet state complex. In the free triplet state, the spin density distribution appears mainly on the carbonyl oxygen and its carbon atom and with a certain amount also on the three ring carbons (C1, C3, and C5). This is consistent with a delocalized nature for the free MAP $\pi\pi^*$ triplet state. In the triplet state complex, the spin density resides predominantly on the ring carbon atoms, particularly the para-substituted groups connecting the C6 and C3 atoms with only a small amount located on the carbonyl moiety. This indicates a ring localized π system and a biradical nature for the H-bond $\pi\pi^*$ complex triplet state.

The validity of the calculated geometric and electronic structures for the triplet H-bond complex is also supported by the general agreement between the calculated Raman spectrum (Figure 10d) and the experimental TR^3 spectra obtained in the water mixed MeCN (Figure 10c). Because of the remarkable differences in the vibrational constitution for many of the modes, the frequencies of the experimental features, the related computed values, and their tentative assignments for the triplet complex are given separately in Table 6 from those of the free MAP triplet (shown in Table 3). The computed frequencies of the carbonyl ^{13}C and ^{18}O isotopic substituted complex are also listed in the table to help assign the carbonyl C═O stretching mode. Like many other substituted aromatic compounds,[10,71] the vibrational couplings are extensive for most of the vibrational modes for both the free and the complex triplet states. The assignment descriptions given in Tables 3 and 5 include only vibrations with a predominant contribution to the corresponding modes. The mixed nature of the vibrational modes (especially the ring modes) makes it difficult to correlate directly the frequency differences observed from the spectrum of the free triplet to that of the complex triplet state and also to the related structural changes on going from the free triplet state to the complex triplet state. We therefore discuss only the general features and the most significant differences observed in the spectra of the complex and free triplet.

Comparing the data for the complex and free triplet (see Figure 10 and Tables 4 and 6), one can find that many experimental bands in the complex spectra (Figure 10c,d) have counterparts in the free triplet spectra (Figure 10a,b). However, the other experimental bands are obviously new features or have substantially different normal mode contributions in the complex from the free MAP. These particular features ought to be the spectral manifestation of the configuration alteration caused by the carbonyl H-bond effect. Features of this kind worthy of special attention are the 1331 and 1376 cm^{-1} experimental bands observed in the water mixed solvent. Although these bands appear to be the counterparts of the free 1322 and 1376 cm^{-1} features, respectively, the calculations indicate that they have different vibrational mode makeup and that they are actually different modes. The 1376 cm^{-1} complex feature was calculated to shift-down substantially upon the carbonyl ^{13}C and ^{18}O isotopic substitution, indicating it has a predominate contribution from the carbonyl C═O stretching vibration. This implies that there is some double bond character for the carbonyl group in the triplet state complex consistent with the calculated C═O bond length for the complex triplet state. The 1331 cm^{-1} feature was computed to be mainly sensitive to the ^{13}C substitution and contributed mostly by the $C_{ring}-C_{carbonyl}$ stretching motion. Its counterpart in the free triplet is therefore the 1373 cm^{-1} feature (Table 4). The frequency downshift of this feature is consistent with the calculated weakening of the $C_{ring}-C_{carbonyl}$ bond in going from the free to the complex triplet.

The 1405 cm^{-1} band in the complex spectrum (Figure 10c) was calculated to correspond to a mixed mode related to vibrations of the $C(O)CH_3$ group. Although there appears to be no counterpart for this feature in the free triplet spectrum (Figure 10b), the calculation suggests that the 1186 cm^{-1} free triplet band is from a mode with a similar vibrational makeup. The considerable frequency upshift of this mode agrees with the bond length difference calculated for the complex and free triplet and is consistent with the double versus single-bond-like carbonyl C═O bond for the complex and free triplet, respectively. The obviously enhancement of this feature in the complex as compared to the free triplet spectrum might be associated in someway with the calculated planar versus twisted configuration of the -$C(O)CH_3$ group in the complex and free triplet, respectively. In addition, this together with the other differences in the relative band intensity for the complex and free triplet spectra, might reflect the different resonance enhancements for the two triplets induced by the 416 nm probe wavelength. This is in accordance with the transient absorption study reported by Wirz and co-workers in terms of the different location of the $T_1 \rightarrow T_n$ absorption spectrum recorded in the neat MeCN (λ_{max} = 385 nm) and 50% H_2O/50% MeCN (395 nm).[4a]

From Tables 4 and 6, one can see that, for both the free and the complex triplet states, many experimental features are from modes with contributions from the ring C−C stretching vibrations. The calculated variation of the ring conformation from the complex to free triplet provides an explanation for the experimental frequency shifts observed for these modes. For example, the ring center C−C stretching dominated feature (the Wilson 8a) is observed to upshift from 1569 cm^{-1} in the free triplet to 1596 cm^{-1} in the triplet complex (Figure 8). This can be associated with the computed bond length shortening of the center C−C bond on going from the free to the complex triplet.

One important experimental observation of the present work is that the lifetime of the MAP triplet complex is longer than

TABLE 6: Observed and Calculated Vibrational Frequencies (cm^{-1}) and Tentative Assignments for Triplet State of Carbonyl MAP−H_2O H-Bond Complex

	calculated			
	frequency[a]			
	MAP−H_2O			
experimental	normal	^{13}C	^{18}O	assignment description
579	578 (ν_{21})	578	577	CCC bending (ring)
	648 (ν_{22})	647	647	O(22)−H(23) bending (o.p.) + ring deformation + C(9)−C(10) stretching
	656 (ν_{23})	654	655	ring chair deformation (4) + CC(9)C bending (o.p.)
666	667 (ν_{24})	666	666	HOH(23) bending (o.p.)
	728 (ν_{25})	728	728	C−H bending (o.p., ring)
744	740 (ν_{26})	740	740	C−C stretching (all, mainly ring) + O(7)−C(3>8) stretching + HOH(23) bending (o.p.) + C(10)H3 wag
	776 (ν_{27})	775	776	C−H bending (o.p., ring) + ring deformation
917	895 (ν_{28})	892	891	C−C stretching (ring + C(9)−C(10))
	924 (ν_{29})	921	920	C−C stretching (ring + C(9)−C(10)) + C(10)H3 wag
	942 (ν_{30})	942	942	C−H(18/19) bending (o.p.)
	971 (ν_{31})	971	971	C−H(20/21) bending (o.p.)
	986 (ν_{32})	980	986	C(10)H3 twist + CC(9)C bending (o.p.)
	1002 (ν_{33})	1002	1001	O(7)−C(8) stretching
995	1039 (ν_{34})	1034	1038	C(10)H3 wag + C−C stretching (C(9)−C(10) + ring) + O(7)−C(8) stretching
1108	1089 (ν_{35})	1089	1087	C−C stretching (mainly ring) + C−H(20/21) bending (i.p.) + C(8)H3 wag
	1117 (ν_{36})	1117	1117	C−H bending (i.p., ring) + C(8)H3 wag + C−C stretching (ring)
	1131 (ν_{37})	1131	1131	C(8)H3 twist
1173	1177 (ν_{38})	1177	1177	C(8)H3 wag + C−H bending (i.p., ring)
1191	1184 (ν_{39})	1183	1184	C(8)H3 wag
1282	1277 (ν_{40})	1277	1276	C−C stretching (ring + C(6)−C(9)) + O(7)−C(3>8) stretching + C−H bending (i.p., ring)
1307	1299 (ν_{41})	1294	1298	O(7)−C(3>8) stretching + C−C stretching (all) + C−H bending (i.p., ring) + C(8)H3 wag + C═O stretching
1331	1325 (ν_{42})	1303	1320	C−C stretching (all, major C(6)−C(9)) + C(10)H3 scissor
	1341 (ν_{43})	1336	1340	C−H bending (i.p., ring)
1376	1356 (ν_{44})	1344	1346	C═O stretching + C(9)−C(6/10) stretching + C(10)H3 wag
1405	1366 (ν_{45})	1356	1362	C−C stretching (all, major C(9)−C(10)) + C═O stretching + C−H bending (i.p., ring)
1431	1427 (ν_{46})	1425	1426	C(8)H3 and C(10)H3 deformation + C−H bending (i.p., ring) + C−C stretching (all)
	1444 (ν_{47})	1444	1444	C(10)H3 deformation
	1445 (ν_{48})	1444	1445	C(10)H3 deformation
1455	1454 (ν_{49})	1454	1454	C(8)H3 deformation
	1457 (ν_{50})	1457	1457	C(8)H3 deformation + O(7)−C(3) stretching + C−C stretching (ring + C(6)−C(9)) + C−H bending (i.p., ring)
	1461 (ν_{51})	1461	1461	C(8)H3 deformation + O(7)−C(3) stretching + C−C stretching (ring)
1504	1508 (ν_{52})	1507	1508	C−C stretching (mainly ring)
1596	1629 (ν_{53})	1628	1628	C−C stretching (mainly ring) + C(6)−C(9))
1836				2 ν_{28} (917)

[a] Scaling factor for the calculated frequencies is 0.970. i.p.: in-plane; o.p.: out-of-plane.

that of the free triplet state. We note that many of previous phosphorescence studies on various AC compounds found a similar change of the triplet lifetime in the H-bonding solvent versus a nonpolar or polar aprotic solvent. This lifetime deviation has been related to the alternation of the triplet electronic configuration ($n\pi^*$ vs $\pi\pi^*$, or a variation in the degree of coupling between the two states) caused by the triplet solute−solvent H-bonding interaction (the H-bonding stabilizes the $\pi\pi^*$ triplet and destabilizes the $n\pi^*$ triplet at the same time).[21,22,24,25] Our result here indicates that, besides the electronic property, the geometric configuration of the triplet can also be altered profoundly by the H-bonding effect, and this structural difference may jointly account for the change of the triplet lifetime. The comparison of the MAP triplet in neat MeCN (free triplet with twisted structure and delocalized $\pi\pi^*$ nature) and water mixed MeCN (H-bonded triplet complex with planar structure and localized $\pi\pi^*$ character) affords an example for such a viewpoint. The data here indicate clearly that, by introducing a H-bond interaction for the carbonyl oxygen with the surrounding water molecule(s), the carbonyl twist coordination can be hindered so that a planar triplet with a longer lifetime can be attained. This triplet structure−lifetime correlation is consistent with the well-established conclusion that out-of-plane distortion of the triplet geometry as compared to the planarity of the ground state is the key factor in influencing the $T_1 \rightarrow S_0$ ISC radiationless transition rate, and the enhancement of Franck−Condon factor resulting from the nonplanar distortion of the triplet has been identified as the primary cause to account for the shortening of the triplet lifetime and a decrease of the phosphorescence yield.[63−67]

Although the formation of the triplet complex containing one AC molecule and a certain amount of solvent (such as water) molecule(s) has been suggested in previous works,[24,25] our work here provides some of the first vibrational spectroscopic evidence to confirm the importance of this H-bonding effect and substantiates the significant differences caused by the H-bond for the triplet structure and lifetime.

E. Triplet H-Bond Effect and the Triplet Reactivity. Extensive investigations reported in the literature indicate that the solute−solvent H-bond has a profound influence on the reactivity of the AC triplet state.[26−28,31,53] However, the mechanism of the related H-bond effect is not well-established. The results here on the identification of the triplet H-bond complex and its remarkable structural and electronic differences from that of the free triplet state can provide an interpretation to some of the observations that have been reported but not well-understood in previous studies. One such example is the photoinduced hydrogen abstraction from phenols by aromatic ketones.

Among various reactions, hydrogen abstraction is the most thoroughly studied photochemical reaction of the AC triplet.[16,17,19,27,31,72] It is well-established that, for aliphatic or benzylic hydrogen abstraction, ketones with the lowest $\pi\pi^*$ triplet state are much less reactive than those with the lowest

$n\pi^*$ triplet state. For example, the MAP triplet ($\pi\pi^*$ nature) was found to be 10−100 times less reactive than benzophenone ($n\pi^*$ triplet) toward hydrogen abstraction from alcohols and hydrocarbons.[16] Besides, the $\pi\pi^*$ triplet reactivity of this kind has been described in terms of the participation of an equilibrium population of the nearby upper $n\pi^*$ triplet,[16,27] although some groups favored the vibronic coupling origination of the close-lying $n\pi^*$ and $\pi\pi^*$ triplet states.[17,19] A mechanism of this kind of hydrogen abstraction reaction is based on the alkoxy radical character of the $n\pi^*$ triplet.[16,72] However, for the hydrogen abstraction from phenols, the reactions were observed to occur at rate of near diffusion-controlled value and were found to be independent of the nature of the ketone triplet (i.e., $\pi\pi^*$ vs $n\pi^*$).[20,27,53] Convincing time-resolved experimental evidence has been presented that supports a reaction mechanism involving a coupled electron/proton transfer within a putative carbonyl H-bonded triplet complex containing the ketone molecule of interest and a phenol molecule. One interesting observation for this reaction between MAP and phenols is that the presence of water in the solution system leads to a retarding influence on the rate of the bimolecular reaction.[53] This effect is also observed for hydrogen abstraction by other $\pi\pi^*$ aromatic ketone triplet states.[27,73] Although this has been explained by some groups in terms of a decrease in the concentration of the free phenol through H-bonding with solvent water molecules,[53] our result here implies that formation of the ketone triplet carbonyl H-bond complex with water molecule(s) could be another important reason to account for the reduced triplet reactivity since the carbonyl H-bond with water can compete effectively with the carbonyl H-bond to the phenols due to the extraordinary H-bond donating ability of the water molecules. This is especially true since there has been no reduced reactivity observation for the $n\pi^*$ nature triplet state.

As mentioned in the Introduction, MAP is the model compound of the *p*MP caged phototriggers. The triplet H-bond effect observed here in the water containing solvents provides an improved insight into understanding the deprotection mechanism of the *p*MP and the closely related *p*HP phototriggers. The triplet states of *p*MP and *p*HP (the free triplets as those observed in MeCN) have been identified to be both $\pi\pi^*$ in nature with similar structures.[1,3,10,13,16,27,30] The methoxy and hydroxy groups are electron donors with similar strength, and they are expected to have similar electronic effects in the triplet state. This implies that, like the case of MAP in 50% H_2O/50% MeCN, the HP triplet may exist also in the form of the carbonyl H-bonded complex in aqueous containing solution. This could apply also to the corresponding *p*MP and *p*HP phototriggers. However, the H-bonding and its influence on the triplet configuration are highly sensitive to charge density of the carbonyl oxygen that could be affected by the presence of leaving groups. Thus, the details of the structures of the triplet H-bonded complex for these phototriggers and their differences from that of the model MAP complex require further investigation. Even so, it is reasonable to think that the photorelease reaction of the *p*HP caged phototriggers in aqueous solution occurs in the triplet manifold[9,10] with the carbonyl H-bonded complex as a reactive precursor. As the H-bonding configuration is considered to be similar for the corresponding *p*MP and *p*HP phototriggers, the previous results for the absence of the photorelease reaction for the *p*MP caged acetate (*p*MPA) versus the efficient photodeprotection of the *p*HP caged acetate (*p*HPA) in 50% H_2O/50% MeCN[6] implies that the hydroxy group plays a crucial role in the *p*HP deprotection processes. Since both the phototriggers contain the same acetate leaving group, this means also that the direct cleavage of the C−O bond connecting the cage and leaving group could not be the major mechanism accounting for the photorelease reaction, at least for the acetate leaving group case. This point is also confirmed by the situation where the leaving group is diethyl phosphate[1,3] and indicates indirectly that the observed photoreactions of *p*-methoxyphenacyl diethyl phosphate in organic solvents such as dioxane and methanol[1] might occur through a mechanism other than the one for the *p*HP caged phototriggers. It is interesting to mention in this regard that, although the triplet can form H-bond with solvent water molecule(s), the same may not apply when the solvent is changed to other alcohol solvents.[24]

The additional reactivity of the hydroxy as compared to the methoxy compound is the rapid deprotonation of the former in the triplet state leading to the formation of the corresponding base that has been suggested to have some charge-transfer character.[4a,6,74] In the triplet carbonyl H-bond complex where the phenyl ring already has some quinonoid character as described in preceding sections, the hydroxy deprotonation might induce a proton transfer of the H-bonded water hydrogen to the carbonyl oxygen and facilitate the generation of a quinone methide (QM) intermediate in the triplet manifold. A mechanistic study of the *p*HPA photodeprotection performed by Wan and co-workers suggest that the QM species (but in the singlet manifold) is the key reactive transient responsible for the photorelease chemistry.[6] However, DFT calculations performed by Wirz and co-workers found that the estimated triplet energy of QM is far too low to enable it to expel a leaving group (the energy of the singlet QM is even lower). They therefore considered the argument for the QM as a reactive intermediate being very improbable and proposed an alternative direct triplet cleavage pathway for the *p*HP photodeprotection based on a picosecond transient absorption experiment on the *p*HP caged phosphate.[4a] Up to now, there has not been solid enough spectroscopic evidence to clearly evaluate these two mechanistic arguments. Further time-resolved work is undergoing in this lab, aiming to identify the involved intermediates and establish the dynamic order of these species. This will help to provide a clearer overall description for the *p*HP deprotection processes and hopefully clarify the previous controversy on the deprotection mechanism.

Conclusion

TR^3 spectroscopy in the picosecond and nanosecond time domain combined with DFT calculations have been performed to characterize the structure, dynamics, and H-bonding effect on the triplet state of the phototrigger model compound MAP in cyclohexane, MeCN, and 50% H_2O/50% MeCN mixed solvent. Comparison of the experimental and DFT work has also been done to study the corresponding properties of the ground state MAP. In 50%,H_2O/50%,MeCN solvent, both the ground state and the triplet state have been found to be strongly associated with the solvent water molecule(s) as H-bond complexes. To clarify the H-bond interactions and their influence on the geometric and electronic configuration of the ground and triplet MAP, the calculations of the optimized geometries, the H-bond interaction energies, and spin densities (for the triplet) on the isolated free MAP are compared to those of MAP−H_2O H-bond complexes [in which the methoxy and carbonyl oxygens are each H-bonded with one (methoxy and carbonyl) or two waters (carbonyl)]. Among the various configurations, the H-bond at the carbonyl site involving one water molecule was found to be the most stable for both the ground and the triplet state complexes with the triplet carbonyl H-bond being stronger

than the corresponding ground state. This is consistent with the increased basicity of the MAP $\pi\pi^*$ triplet suggested in previous investigations in the literature. The calculated Raman spectrum of the ground and triplet state of the free MAP and carbonyl H-bond MAP−H_2O complex reproduces reasonably well the normal Raman (for the ground state) and TR^3 (for the triplet state) spectra obtained in neat MeCN and 50% H_2O/50% MeCN solvent, respectively. This supports the H-bond complex model and indicates that the carbonyl H-bond is responsible for the spectral difference observed in the two solvents. The structure of the ground state free and carbonyl H-bond complex are both planar in terms of the relative orientation between the ring and the carbonyl related -$C(O)CH_3$ group but with the C═O bond length lengthened slightly due to the carbonyl H-bond effect in the complex. The triplet of the free MAP has a slightly twisted geometry with a delocalized $\pi\pi^*$ character and a single-bond-like carbonyl group. The triplet of the H-bond complex, on the other hand, was calculated to be planar in structure with a significant ring localized biradical $\pi\pi^*$ nature and a double-band-like carbonyl group.

From the temporal evolution of the triplet TR^3 spectra, it was found that the triplet of both the free MAP and the carbonyl H-bond complex is generated rapidly after photoexcitation. The early picosecond dynamics of the Raman bandwidth and frequency changes are due to the relaxation of excess energy of the initially formed energetic triplet state. Monoexponential decays were observed for both the free triplet state and the triplet state of the H-bond complex. The latter implies that there is no dissociation of the H-bond complex back to the free triplet over this time period and reflects the strong H-bond interaction between the MAP and the solvent water molecule in the triplet manifold. The lifetime of the free triplet state and the complex triplet state were measured to be 40 ns and 160 ns, respectively. The longer lifetime of the complex triplet state than that of the free triplet state was associated with the structural differences in terms of the twisted versus planar conformation calculated for the free and complex triplet states, respectively. On the basis of the rapid ISC rate ($\sim 5 \times 10^{11}$ s^{-1}), the triplet of the H-bond complex was suggested to be produced directly from the corresponding ground state complex that was found to be the predominant ground state species in the water mixed solvent. The implication of the carbonyl H-bond effect on the triplet reactivity has been discussed briefly in regards to the photodeprotection reactions of the *p*MP and *p*HP caged phototriggers and some other related triplet state reactions reported in previous studies in the literature.

Acknowledgment. We thank the Research Grants Council of Hong Kong (HKU 7108/02P and HKU 1/01C) to D.L.P. for support of this research. W.M.K. thanks the University of Hong Kong for the award of a Research Assistant Professorship.

Supporting Information Available: Details for calculated structures and Raman spectra of the ground and triplet state of various MAP−water complexes. This material is available free of charge via the Internet at http://pubs.acs.org.

References and Notes

(1) (a) Givens, R. S.; Kueper, L. W. *Chem. Rev.* **1993**, *93*, 55−66 and references therein. (b) Givens, R. S.; Athey, P. S.; Matuszewski, B.; Kueper, L. W., III; Xue, J. Y.; Fister, T. *J. Am. Chem. Soc.* **1993**, *115*, 6001−6012 and references therein. (c) Gee, K. R.; Kueper, L. W., III; Barnes, J.; Dudley, G.; Givens, R. S. *J. Org. Chem.* **1996**, *61*, 1228−1233.

(2) Givens, R. S.; Athey, P. S.; Kueper, L. W., III; Matuszewski, B.; Xue, J.-Y. *J. Am. Chem. Soc.* **1992**, *114*, 8708−8710.

(3) (a) Gives, R. S.; Park, C.-H. *Tetrahedron Lett.* **1996**, *37*, 6259−6262. (b) Park, C.-H.; Givens, R. S. *J. Am. Chem. Soc.* **1997**, *119*, 2453−2463. (c) Givens, R. S.; Jung, A.; Park, C.-H.; Weber, J.; Bartlett, W. *J. Am. Chem. Soc.* **1997**, *119*, 8369−8370. (d) Givens, R. S.; Weber, J. F. W.; Conrad, P. G., II; Orosz, G.; Donahue, S. L.; Thayer, S. A. *J. Am. Chem. Soc.* **2000**, *122*, 2687−2697 and references therein. (e) Conrad, P. G., II; Givens, R. S.; Weber, J. F. W.; Kandler, K. *Org. Lett.* **2000**, *2*, 1545−1547.

(4) (a) Conrad, P. G., II; Givens, R. S.; Hellrung, B.; Rajesh, C. S.; Ramseier, M.; Wirz, J. *J. Am. Chem. Soc.* **2000**, *122*, 9346−9347. (b) Il'ichev, Y. V.; Schworer, M. A.; Wirz, J. *J. Am. Chem. Soc*. **2004**, *126*, 4581−4595. (c)Rajesh, C. S.; Givens, R. S.; Wirz, J. *J. Am. Chem. Soc.* **2000**, *122*, 611−618. (d) Hangarter, M.-A.; Hörmann, A.; Kamdzhilov, Y.; Wirz, J. *Photochem. Photobiol. Sci.* **2003**, *2*, 524−535.

(5) (a) Banerjee, A.; Falvey, D. E. *J. Am. Chem. Soc.* **1998**, *120*, 2965−2966. (b) Lee, K.; Falvey, D. E. *J. Am. Chem. Soc.* **2000**, *122*, 9361−9366. (c) Banerjee, A.; Lee, K.; Yu, Q.; Fan, A. G.; Falvey, D. E. *Tetrahedron Lett.* **1998**, *39*, 4635−4638. (d) Banerjee, A.; Falvey, D. E. *J. Org. Chem.* **1997**, *62*, 6245−6251.

(6) (a) Zhang, K.; Corrie, J. E. T.; Munasinghe, V. R. N.; Wan, P. *J. Am. Chem. Soc.* **1999**, *121*, 5625−5632. (b) Brousmiche, D. W.; Wan, P. *J. Photochem. Photobiol., A* **2000**, *130*, 113−118.

(7) Namiki, S.; Arai, T.; Fujimori, K. *J. Am. Chem. Soc.* **1997**, *119*, 3840−3841.

(8) Sheehan, J. C.; Umezawa, K. *J. Org. Chem.* **1973**, *38*, 3771−3774.

(9) Ma, C.; Kwok, W. M.; Chan, W. S.; Zuo, P.; Kan J. T. W.; Toy, P. H.; Phillips, D. L. *J. Am. Chem. Soc.* **2005**, *127*, 1463−1427.

(10) (a) Ma, C.; Chan, W. S.; Kwok, W. M.; Zuo, P.; Phillips, D. L. *J. Phys. Chem. B*, **2004** *108*, 9264−9276. (b) Ma, C.; Zuo, P.; Kwok, W. M.; Chan, W. S.; Kan, J. T. W.; Toy, P. H.; Phillips, D. L. *J. Org. Chem.* **2004**, *69*, 6641−6657.

(11) Kwok, W. M.; George, M. W.; Grills, D. C.; Ma, C.; Matousek, P.; Parker, A. W.; Phillips, D.; Toner, W. T.; Towrie, M. *Angew. Chem., Int. Ed.* **2003**, *42*, 1826−1830.

(12) (a) Bhasikuttan, A. C.; Singh, A. K.; Palit, D. K.; Sapre, A. V.; Mittal, J. P. *J. Phys. Chem. A* **1998**, *102*, 3470−3480. (b) Singh, A. K.; Bhasikuttan, A. C.; Palit, D. K.; Mittal, J. P. *J. Phys. Chem. A* **2000**, *104*, 7002−7009.

(13) (a) Kearns, D. R.; Case, W. A. *J. Am. Chem. Soc.* **1966**, *88*, 5087−5097. (b) Merkel, P. B.; Kearns, D. R. *J. Chem. Phys.* **1973**, *58*, 398−400.

(14) Srivastava, S.; Yourd, E.; Toscano, J. P. *J. Am. Chem. Soc.* **1998**, *120*, 6173−6174.

(15) Lutz, H.; Bréhéret, E.; Lindqvist, L. *J. Phys. Chem.* **1973**, *77*, 1758−1762.

(16) (a) Wagner, P. J.; Kemppainen, A. E.; Schott, H. N. *J. Am. Chem. Soc.* **1973**, *95*, 5604−5614. (b) Wagner, P. J.; Truman, R. J.; Scaiano, J. C. *J. Am. Chem. Soc.* **1985**, *107*, 7093−7097. (c) Wagner, P. J.; Nakahira, T. *J. Am. Chem. Soc.* **1973**, *95*, 8474−8475.

(17) Yang, N. C.; McClure, D. S.; Murov, S. L.; Houser, J. J.; Dusenbery, R. *J. Am. Chem. Soc.* **1967**, *89*, 5466−5468.

(18) Wagner, P. J.; Kemppainen, A. E. *J. Am. Chem. Soc.* **1968**, *90*, 5898−5899.

(19) Yang, N. C.; Dusenbery, R. L. *J. Am. Chem. Soc.* **1968**, *90*, 5899−5900.

(20) Biczók, L.; Béreces, T.; Linschitz, H. *J. Am. Chem. Soc.* **1997**, *119*, 11071−11077.

(21) Rauh, R. D.; Leermakers, P. A. *J. Am. Chem. Soc.* **1968**, *90*, 2246−2249.

(22) Suter, G. W.; Wild, U. P. *J. Phys. Chem.* **1986**, *90*, 2358−2361.

(23) (a) Hoshi, M.; Shizuka, H. *Bull. Chem. Soc. Jpn.* **1986**, *59*, 2711−2715. (b) Shizuka, H.; Kimura, E. *Can. J. Chem.* **1984**, *62*, 2041−2046.

(24) (a) Nakayama, T.; Otani, A.; Hamanoue, K. *J. Chem. Soc. Faraday Trans.* **1995**, *91*, 855−861. (b) Nakayama, T.; Sakurai, K.; Ushida, K.; Hamanoue, K. *J. Chem. Soc., Faraday Trans.* **1991**, *87*, 449−454. (c) Nakayama, T.; Sakurai, K.; Hamanoue K. *J. Chem. Soc., Faraday Trans.* **1991**, *87*, 1509−1512.

(25) Hamanoue, K.; Nakayama, T.; Yamaguchi, T.; Ushida, K. *J. Phys. Chem.* **1989**, *93*, 3814−3818.

(26) Ramseier, M.; Senn, P.; Wirz, J. *J. Phys. Chem. A* **2003**, *107*, 3305−3315.

(27) Das, P. K.; Encinas, M. V.; Scaiano, J. C. *J. Am. Chem. Soc.* **1981**, *103*, 3, 4154−4162.

(28) McGarry, P. F.; Jockusch, S.; Fujiwara, Y.; Kaprinidis, N. A.; Turro, N. J. *J. Phys. Chem. A* **1997**, *101*, 764−767.

(29) (a) Dalton, J. C.; Montgomery, F. C. *J. Am. Chem. Soc.* **1974**, *96*, 6230−6232. (b) Ley, C.; Morlet-Savary, F.; Jacques, P.; Fouassier, J. P. *Chem. Phys.* **2000**, *255*, 335−346. (c) Morlet-Savary, F.; Ley, C.; Jacques, P.; Wieder, F.; Fouassier, J. P. *J. Photochem. Photobiol. A* **1999**, *126*, 7−14.

(30) Bhasikuttan, A. C.; Singh, A. K.; Palit, D. K.; Sapre, A. V.; Mittal, J. P. *J. Phys. Chem. A* **1999**, *103*, 4703−4711.

(31) Scaiano, J. C. *J. Am. Chem. Soc.* **1980**, *102*, 7747−7753.

(32) Kagiya, T.; Sumida, Y.; Inoue, T. *Bull. Chem. Soc. Jpn.* **1968**, *41*, 767−773.

(33) Allerhand, A.; Schleyer, P. v. R. *J. Am. Chem. Soc.* **1963**, *85*, 371−380.
(34) Fuson, N.; Josien, M.; Shelton, E. M. *J. Am. Chem. Soc.* **1954**, *76*, 2526−2533.
(35) Kamlet, M. J.; Abboud, J. M.; Abraham, M. H.; Taft, R. W. *J. Org. Chem.* **1983**, *48*, 2877−2887.
(36) Chudoba, C.; Nibbering, E. T. J.; Elsaesser, T. *J. Phys. Chem. A* **1999**, *103*, 5625−5628.
(37) Hamm, P.; Lim, M.; Hochstrasser, R. M. *Phys. Rev. Lett.* **1998**, *81*, 5326−5329.
(38) Mirkin, N. G.; Krimm, S. *J. Mol. Struct.* **1996**, *377*, 219−234.
(39) Markham, L. M.; Hudson, B. S. *J. Phys. Chem.* **1996**, *100*, 2731−2737.
(40) Alejandro, E.; Fernández, J. A.; Castaño, F. *Chem. Phys. Lett.* **2002**, *353*, 195−203.
(41) Guo, H.; Karplus, M. *J. Phys. Chem.* **1992**, *96*, 7273−7287.
(42) Mirkin, N. G.; Krimm, S. *J. Am. Chem. Soc.* **1991**, *113*, 9742−9747.
(43) Zhan, C.; Chipman, D. M. *J. Phys. Chem. A* **1998**, *102*, 1230−1235.
(44) (a) Mitsui, M.; Ohshima, Y. *J. Phys. Chem. A* **2000**, *104*, 8638−8648. (b) Mitsui, M.; Ohshima, Y. *J. Phys. Chem. A* **2000**, *104*, 8649−8659. (c) Mitsui, M.; Ohshima, Y.; Kajimoto, O. *J. Phys. Chem. A* **2000**, *104*, 8660−8670. (d) Rusakowicz, R.; Byers, G. W.; Leermakers, P. A. *J. Am. Chem. Soc.* **1971**, *93*, 3263−3266.
(45) (a) Kwok, W. M.; Zhao, C.; Li, Y. L.; Guan, X.; Phillips, D. L. *J. Chem. Phys.* **2004**, *120*, 3323−3332. (b) Kwok, W. M.; Zhao, C.; Li, Y.-L.; Guan, X.; Wang, D.; and Phillips, D. L. *J. Am. Chem. Soc.* **2004**, *126*, 3119−3131. (c) Kwok, W. M.; Zhao, C.; Guan, X.; Li, Y. L.; Du, Y.; Phillips, D. L. *J. Chem. Phys.* **2004**, *120*, 9017−9032.
(46) (a) Guan, X.; Du, Y.; Li, Y.-L.; Kwok, W. M.; Phillips, D. L. J. *Chem. Phys.* **2004**, *121*, 8399−8409. (b) Kwok, W. M.; Chan, P. Y.; Phillips, D. L. *J. Phys. Chem. B* **2004**, *108*, 19068−19075.
(47) Frisch, M. J.; Trucks, G. W.; Schlegel, H. B.; Scuseria, G. E.; Robb, M. A.; Cheeseman, J. R.; Zakrzewski, V. G.; Montgomery, J. A., Jr.; Stratmann, R. E.; Burant, J. C.; Dapprich, S.; Millam, J. M.; Daniels, A. D.; Kudin, K. N.; Strain, M. C.; Farkas, O.; Tomasi, J.; Barone, V.; Cossi, M.; Cammi, R.; Mennucci, B.; Pomelli, C.; Adamo, C.; Clifford, S.; Ochterski, J.; Petersson, G. A.; Ayala, P. Y.; Cui, Q.; Morokuma, K.; Malick, D. K.; Rabuck, A. D.; Raghavachari, K.; Foresman, J. B.; Cioslowski, J.; Ortiz, J. V.; Baboul, A. G.; Stefanov, B. B.; Liu, G.; Liashenko, A.; Piskorz, P.; Komaromi, I.; Gomperts, R.; Martin, R. L.; Fox, D. J.; Keith, T.; Al-Laham, M. A.; Peng, C. Y.; Nanayakkara, A.; Gonzalez, C.; Challacombe, M.; Gill, P. M. W.; Johnson, B.; Chen, W.; Wong, M. W.; Andres, J. L.; Gonzalez, C.; Head-Gordon, M.; Replogle, E. S.; Pople, J. A. *Gaussian 98*, *Rev. A7*; Gaussian, Inc., Pittsburgh, PA, 1998.
(48) Reichardt, C. *Solvent and Solvent Effect in Organic Chemistry*; VCH Verlagsgesellschaft mbH, D-6940: Weinheim, 1988.
(49) Besnard, M.; Cabaco, M. I. *Chem. Phys.* **1992**, *163*, 103−114.
(50) Woutersen, S.; Mu, Y.; Stock, G.; Hamm, P. *Chem. Phys.* **2001**, *266*, 137−147.
(51) Oxtoby, D. W.; Levesque, D.; Weis, J.-J. *J. Chem. Phys.* **1978**, *68*, 5528−5533.
(52) Stenger, J.; Madsen, D.; Hamm, P.; Nibbering, E. T. J.; Elsaesser, T. *Phys. Rev. Lett.* **2001**, *87*, 027401-1-4.
(53) (a) Lathioor, E. C.; Leigh, W. J.; St. Pierre, M. J. *J. Am. Chem. Soc.* **1999**, *121*, 11984−11992. (b) Leigh, W. J.; Lathioor, E. C.; St. Pierre, M. J. *J. Am. Chem. Soc.* **1996**, *118*, 12339−12348.
(54) Burgt, M. J. van der; Huizer, A. H.; Varma, C. A. G. O.; Wagner, B. D.; Lusztyk, J. *Chem. Phys.* **1995**, *201*, 525−538.
(55) Ma, C.; Kwok, W. M.; Matousek, P.; Parker, A. W.; Phillips, D.; Toner, W. T.; Towrie, M. *J. Raman Spectrosc.* **2001**, *32*, 115−123.
(56) Matousek, P.; Parker, A. W.; Towire, M.; Toner, W. T. *J. Chem. Phys.* **1997**, *107*, 9807−9817.
(57) Iwata, K.; Hamaguchi, H. J. *J. Phys. Chem. A* **1997**, *101*, 632−637.
(58) Hester, P. E.; Matousek, P.; Moore, J. N.; Parker, A. W.; Toner, W. T.; Towire, M. *Chem. Phys. Lett.* **1993**, *208*, 471−478.
(59) Weaver, W. L.; Huston, L. A.; Iwata, K. Gustafson, T. L. *J. Phys. Chem.* **1992**, *96*, 8956−8961.
(60) Rentzepis, P. M. *Science* **1970**, *169*, 239−247.
(61) Berger, M.; Steel, C. *J. Am. Chem. Soc.* **1975**, *97*, 4817−4821.
(62) Kiritani, M.; Yoshii, T.; Hirota, N. *J. Phys. Chem.* **1994**, *98*, 11265−11268.
(63) (a) Lim, E. C.; Li, Y. H.; Li, R. *J. Chem. Phys.* **1970**, *53*, 2443−2448. (b) Li, R.; Lim, E. C. *J. Chem. Phys.* **1972**, *57*, 605−612. (c) Li, Y. H.; Lim, E. C. *Chem. Phys. Lett.* **1970**, *7*, 15−18.
(64) Koyanagi, M.; Zwarich, R. J.; Goodman, L. *J. Chem. Phys.* **1972**, *56*, 3044−3060.
(65) Ohmori, N.; Suzuki, T.; Ito, M. *J. Phys. Chem.* **1988**, *92*, 1086−1093.
(66) (a) Case, W. L.; Kearns, D. R. *J. Chem. Phys.* **1970**, *52*, 2175−2191. (b) Kearns, D. R.; Case, W. A. *J. Am. Chem. Soc.* **1966**, *88*, 5087−5097.
(67) (a) Lim, E. C. *J. Phys. Chem.* **1986**, *90*, 6770−6777. (b) Hirata, Y.; Lim, E. C. *J. Chem. Phys.* **1980**, *73*, 3804−3809. (c) Hirata, Y.; Lim, E. C. *J. Chem. Phys.* **1980**, *72*, 5505−5510.
(68) Tanaka, S.; Kato, C.; Horie, K.; Hamaguchi, H. *Chem. Phys. Lett.* **2003**, *381*, 385−391.
(69) Tahara, T.; Hamaguchi, H.; Tasumi, M. *J. Phys. Chem.* **1990**, *94*, 170−178.
(70) Case, W. A.; Kearns, D. R. *J. Chem. Phys.* **1970**, *52*, 2175−2191.
(71) (a) Kwok, W. M.; Ma, C.; George, M. W.; Grills, D. C.; Matousek, P.; Parker, A. W.; Phillips, D.; Toner, W. T.; Towrie, M. *Phys. Chem. Chem. Phys.* **2003**, *5*, 1043−1050. (b) Kwok, W. M.; Ma, C.; Matousek, P.; Parker, A. W.; Phillips, D.; Toner, W. T.; Towrie, M.; Umapathy, S. *J. Phys. Chem. A* **2001**, *105*, 984−990.
(72) Turro, N. J. *Modern Molecular Photochemistry*; University Science Books: Sausalito, California, 1991.
(73) Evans, C.; Scaiano, J. C.; Ingold, K. U. *J. Am. Chem. Soc.* **1992**, *114*, 4589−4593.
(74) Porter, G.; Suppan, P. *Trans. Faraday Soc.* **1965**, *61*, 1664−1673.